Fluid flow near reservoir lakes inferred from the spatial and temporal analysis of the electric potential

Michaël Trique,[1] Frédéric Perrier, Thierry Froidefond, and Jean-Philippe Avouac
Département Analyse, Surveillance, Environnement, Commissariat à l'Energie Atomique, Bruyères-Le-Châtel, France

Sophie Hautot
UMR 6538 "Domaines Océaniques", IUEM Technopole Brest-Iroise, Plouzané, France

Received 16 February 2001; revised 16 May 2002; accepted 16 May 2002; published 19 October 2002.

[1] Electric self-potential (SP) variations have been monitored continuously from 1995 to 1998 at 14 points on a ridge separating the Roselend and La Gittaz reservoir lakes in the French Alps. The lakes have level variations of at least 50 m over yearly cycles. Seasonal variations of SP associated with lake-level variations are observed on five points of the array. For three points located on the banks of the lakes, a positive correlation to the lake-level variations is observed with a maximal amplitude of about 180 mV, corresponding to an average response of 2.4 mV per meter of water. For two points located on the bottom of each lake, the correlation is negative, with a maximal magnitude of about −50 mV, corresponding to an average response of −1.1 mV per meter of water. Two independent temporary electrical arrays located on the banks of each lake confirm these measurements and allow a better spatial characterization of the sources associated with the observed SP variations. In particular, near the Roselend lake, the electrical response to lake-level variations is increasing for decreasing altitude. The measured SP variations are proposed to result from the electrokinetic coupling associated with a vertical groundwater flow connecting a constant pore pressure source to the bottom of the lakes. Numerical modeling indicates that the spatial variation of the response and the nonlinear response observed at one point can be explained by leakage currents in the conductive lake water. The values of the streaming potential coefficient (SPC), measured in the laboratory with crushed rock samples from the site, range from 14 to 50 mV/0.1 MPa for an electrolyte resistivity of 40 Ω m and are compatible, to first order, with the magnitude of the observed seasonal SP variations. A detailed quantitative electrokinetic modeling is currently limited mainly by the poor knowledge on the contribution of electrical leakage currents and the local variability of the SPC. This experiment indicates that spatial and temporal variations of the electric potential are promising tools to characterize and monitor shallow groundwater flow and provide practical data for the investigation of groundwater flow associated with volcanic or tectonic activity. *INDEX TERMS:* 1832 Hydrology: Groundwater transport; 7223 Seismology: Seismic hazard assessment and prediction; 0925 Exploration Geophysics: Magnetic and electrical methods; 8424 Volcanology: Hydrothermal systems (8135); *KEYWORDS:* self-potential; streaming potential; electrokinetic effect; earthquake precursors; groundwater circulation; magnetotellurics

Citation: Trique, M., F. Perrier, T. Froidefond, J.-P. Avouac, and S. Hautot, Fluid flow near reservoir lakes inferred from the spatial and temporal analysis of the electric potential, *J. Geophys. Res.*, *107*(B10), 2239, doi:10.1029/2001JB000482, 2002.

1. Introduction

[2] Detecting subsurface groundwater circulation using geophysical methods is an important issue for the evaluation of water resources and waste management [e.g., *Aubert and Yéné Atananga*, 1996; *Harvey et al.*, 1997] or the understanding of phenomena associated with volcanic or tectonic activity. Fluid flow indeed has been shown to play an important role in the seismic cycle. For example, the release of large amounts of water has been observed after large earthquakes [*Muir-Wood and King*, 1993] and fluid flow accounts for the time distribution of aftershocks [*Nur and Booker*, 1972] or earthquake sequences [*Noir et al.*, 1997]. Fluid flow may also play an important role in the earthquake preparation phase [*Scholz et al.*, 1973; *Roeloffs*, 1988; *Koizumi et al.*, 1999].

[3] Through the electrokinetic effect (EKE), fluid flow in rocks can generate measurable electrical signals, referred to

[1]Now at European Patent Office, Munich, Germany.

0148-0227/02/2001JB000482$09.00

as streaming potentials. Following early studies with porous materials, the EKE has now been studied in detail in the laboratory with rock samples [*Ishido and Mizutani*, 1981; *Morgan et al.*, 1989; *Jouniaux and Pozzi*, 1995a, 1995b; *Lorne et al.*, 1999a, 1999b; *Jouniaux et al.*, 2000]. In particular, variations of the amplitude of the streaming potential coefficient (SPC) are observed during the deformation and before the rupture of saturated sandstone [*Jouniaux and Pozzi*, 1995a, 1995b; *Yoshida et al.*, 1998; *Lorne et al.*, 1999a, 1999b]. Such laboratory measurements have helped in developing a better understanding of the EKE in geophysical systems [*Lorne et al.*, 1999a, 1999b; *Revil et al.*, 1999a, 1999b].

[4] In the field, the EKE is often proposed to explain static self-potential (SP) anomalies. For example, SP anomalies observed in reservoir lakes or on earth dams were attributed to the EKE associated with water leakage from the reservoir [*Ogilvy et al.*, 1969; *Bogoslovsky and Ogilvy*, 1970; *Gex*, 1980]. The large positive anomalies (sometimes larger than 1 V) reported in volcanic areas [*Malengreau et al.*, 1994; *Zlotnicki et al.*, 1994; *Hashimoto and Tanaka*, 1995; *Ishido et al.*, 1997; *Sasai et al.*, 1997; *Lénat et al.*, 1998; *Michel and Zlotnicki*, 1998] and geothermal fields [*Zohdi et al.*, 1973; *Corwin and Hoover*, 1979; *Revil and Pezard*, 1998; *Revil et al.*, 1999b] are associated through the EKE with the hydrothermal activity along fractured zones. The EKE is also invoked to explain the temporal variations of the geomagnetic field [*Zlotnicki and Le Mouël*, 1988; *Zlotnicki and Le Mouël*, 1990] or temporal variations of SP observed before a volcanic eruption [e.g., *Fujinawa et al.*, 1992; *Sasai et al.*, 2001; *Zlotnicki et al.*, 2001]. The existence of the EKE in natural systems is also demonstrated by the temporal variations of SP associated with periodic spring discharge [*Perrier et al.*, 1999], with subglacial water pressure field variations [*Blake and Clarke*, 1999] or with stress changes in quarries [*Morat et al.*, 1989; *Morat and Le Mouël*, 1992; *Gensane et al.*, 1999]. In soils, SP variations can occur in association with shallow water circulation in the nonsaturated zone [*Thony et al.*, 1997; *Perrier and Morat*, 2000].

[5] Despite this body of experimental results, several questions remain. First, the relationship between laboratory results and field effects remains poorly known. In addition, most of these experiments were performed at small scales, of the order of one meter or less in some cases [*Gensane et al.*, 1999]. Investigating the relevance of the EKE at crustal scales (larger than 1 km at least) is however extremely important. Beyond the SP variations associated with volcanic eruptions mentioned above, electrical effects associated with the preparation of an earthquake may lead to earthquake precursors [*Corwin and Morrison*, 1977; *Park et al.*, 1993; *Raleigh et al.*, 1977; *Varotsos et al.*, 1993, 1999], through the EKE [*Mizutani et al.*, 1976] or other mechanisms [e.g., *Yoshida et al.*, 1998; *Varotsos et al.*, 1999]. However, no convincing evidence to support or disprove this hypothesis could be presented [e.g., *Geller*, 1996, 1997; *Lighthill*, 1996]. To contribute to resolving this issue, it appears important to understand better the relationship between rock deformation, fluid flow, and SP at the kilometer scale.

[6] In order to investigate these questions, we set up in 1995 an experiment in the French Alps in the vicinity of two reservoir lakes, Roselend and La Gittaz. These lakes are characterized by yearly level variations of the order of 50 m or more and thus provide significant hydrogeological and mechanical perturbations. Electrical measurements were performed on the Sur-Frêtes ridge separating these two lakes, using 20 dipoles with length varying from 50 m to about 2 km. We first observed, at one point close to the Roselend lake, unambiguous SP variations associated with the yearly level variations [*Perrier et al.*, 1998]. This signal was interpreted by an EKE induced by groundwater flow forced by the lake level. In addition, transient electrical signals were recorded at one point of the ridge in association with transient deformation and radon emanation observed in a tunnel located near the Roselend dam [*Trique et al.*, 1999].

[7] Here, we report more detailed observations of seasonal variations of SP at the Sur-Frêtes site. We present a complete set of spatial and temporal SP variations. In addition, seasonal variations of the amplitude of the MT signals were observed to be related to the level variations of the reservoir lakes. Additional results concerning the transient geophysical signals associated with transient deformation will be presented in a separate paper [Perrier et al., in preparation, 2002].

2. Description of the Experiment

2.1. General Description of the Site

[8] The Sur-Frêtes ridge is located in the French Alps, 30 km south-west of the Mont Blanc, at the geological contact between the Belledonne crystalline basement to the west and highly tectonized permo-triassic units to the east, overthrust by Jurassic sheets (Figure 1). The main contacts separating the different geological units have dip angles varying from 35°E to subvertical with a N30°E strike. The ridge, oriented in the east-west direction with an elevation varying between 1792 and 1826 m, separates the Roselend basin in the south from the La Gittaz basin in the north, and presents a topographic slope of about 25° and 40° on the southern and northern sides, respectively.

[9] The Roselend lake, which has a capacity of 183×10^6 m^3 and a maximal altitude of 1557 m, communicates through an underground water pipe with the smaller La Gittaz lake, which has a capacity of 13×10^6 m^3 and a maximal altitude of 1562 m. The two lakes collect the water from a natural drainage basin of 55 km^2 and from 206 km^2 of neighboring drainage basins through an array of underground galleries [*Janod*, 1957]. The two dams are set against the crystalline rocks (Figure 1).

[10] The lake level cycle, which slightly varies from year to year, is correlated to the meteorological cycle only during the snow melting period from late spring to summer. From December to May, the site is covered by snow. During the winter, the lakes are emptied according to the needs of electricity power production, the main power station (550 MW) being located in Albertville, 14 km west of the site. A small power station (18 MW), located one km south east of the Sur-Frêtes ridge at the input of the Roselend lake, has no observed significant impact on the seasonal component of SP. The amplitude of the water level yearly cycle ranges from 50 to 70 m for the Roselend lake and from 35 to 50 m for the La Gittaz lake. The regular pattern of the yearly

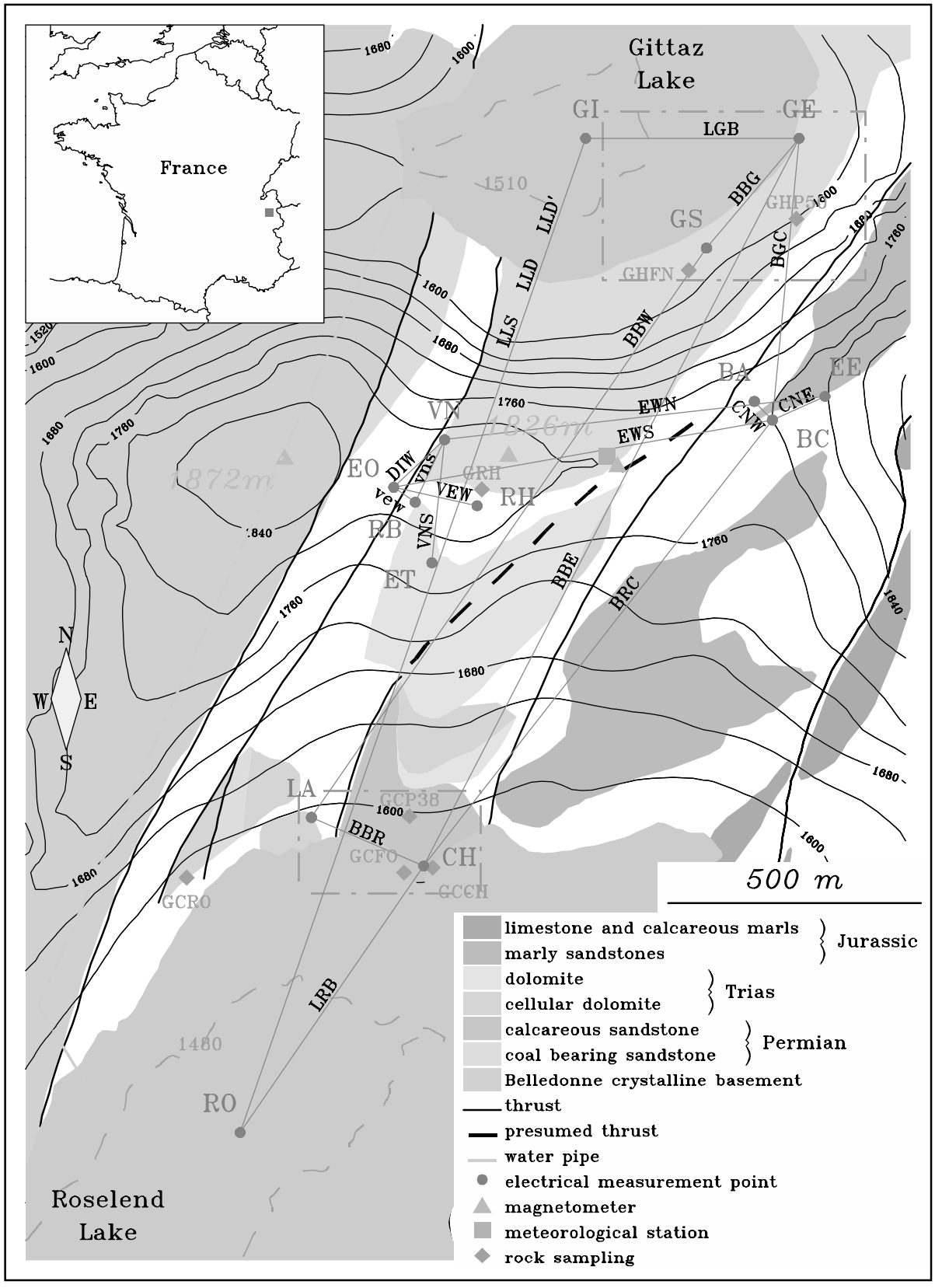

Figure 1. Map of the Sur-Frêtes ridge with the main geological units and the permanent SP monitoring array. The locations of rocks sampled for laboratory measurements are also indicated. See color version of this figure at back of this issue.

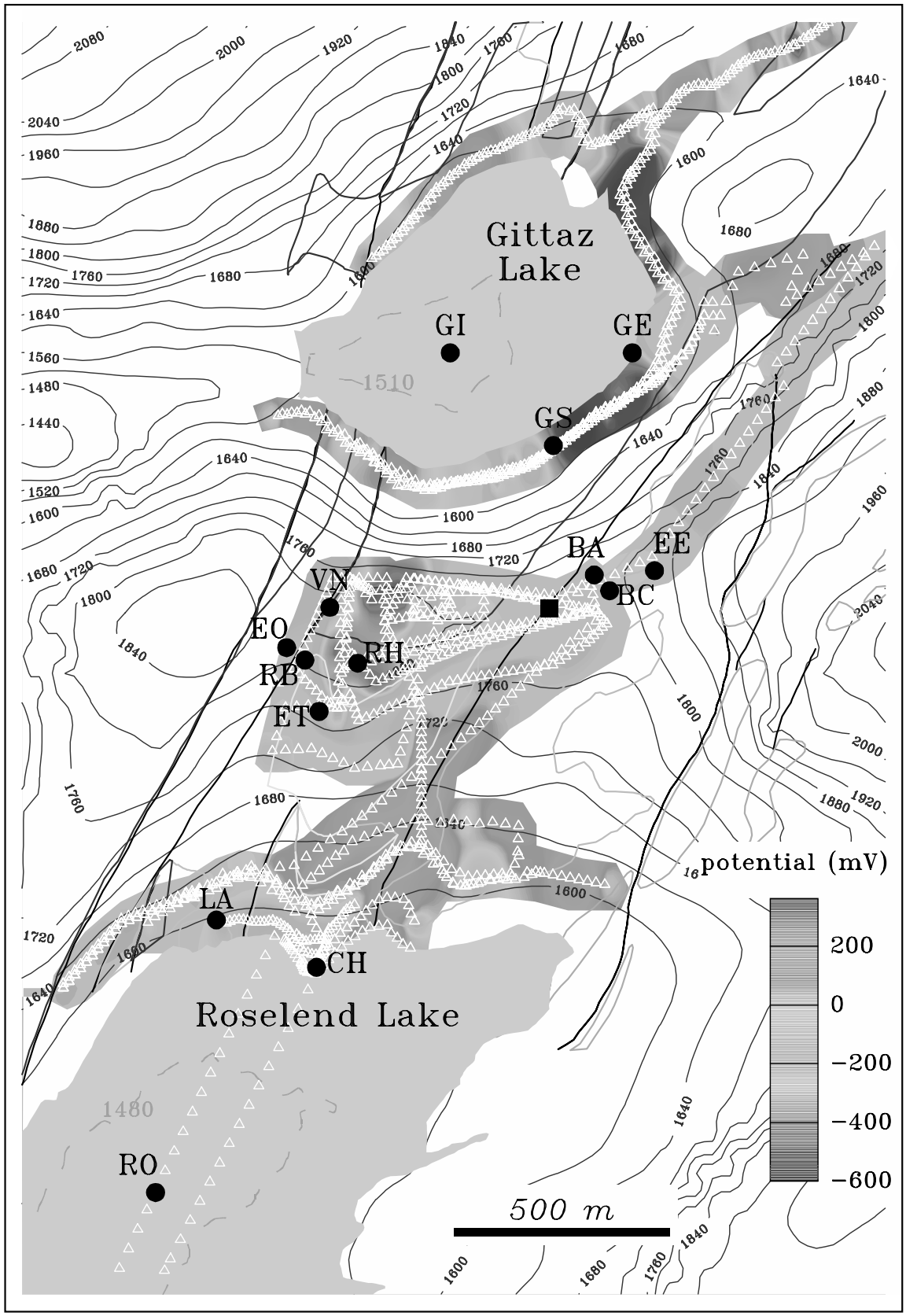

Figure 2. Map of the static SP distribution. The SP measurement points are indicated by white triangles (approximately a total of 1300 points). The contours of the main geological units are displayed using the color code defined in Figure 1. The reference point for the SP mapping is represented by a black square. The black dots represent the measurement points of the permanent SP monitoring array. See color version of this figure at back of this issue.

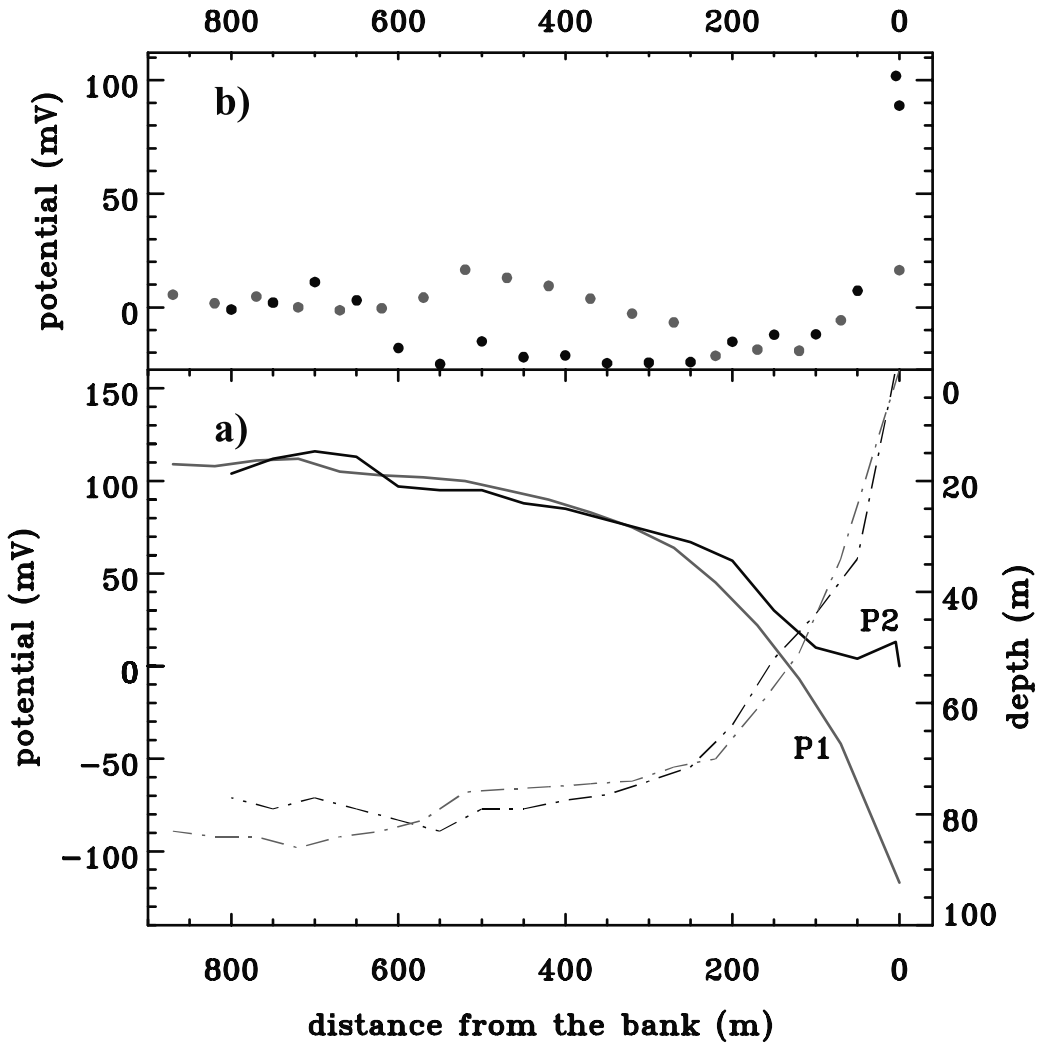

Figure 3. (a) Static SP profiles P1 (gray line) and P2 (black line) performed on the bottom of the Roselend lake (Figure 2) as a function of the horizontal distance to the bank. The corresponding depth in water (dashed line) is indicated on the scale on the right side. (b) P1 and P2 SP profiles results corrected for topography with a linear factor of 2.8 and 2.5 mV/m, respectively.

water level cycles is essential to assess the reproducibility of the electrical measurements.

2.2. Characterization of the Static Electric Potential

[11] The characterization of the static SP distribution has been performed on four different areas of the site: the Sur-Frêtes ridge (September–October 1995), the area around the La Gittaz lake (September–October 1995 and July 1997), the northern part of the bank of the Roselend lake (September–October 1995 and July 1997) and the northern part of the bottom of the Roselend lake (September 1998). The experimental methods are described in appendix A and the results are presented in Figures 2, 3, and 4.

[12] The SP with respect to the BC point, taken as reference, ranges from −600 to +300 mV (Figure 2). No clear relation to topography is observed on this site, although SP is frequently dominated by a topographic component [*Corwin and Hoover*, 1979; *Ernston and Scherer*, 1986]. However, the SP on the P1 profile, located on the bottom of the Roselend lake, is rising with increasing depth with a ratio of about 2.8 mV per meter depth (Figure 3a). The deviation of the electric potential from this trend does not exceed 20 mV (Figure 3b). For the P2 profile, this behavior is observed only between 30 and 90 m depth, with a ratio of about 2.5 mV per meter depth, whereas the electric potential does not vary by more than 15 mV above the depth of 30 m. In this case, the deviation from the linear trend exceeds 20 mV and reaches 120 mV only above 30 m depth (Figure 3b).

[13] Three negative anomalies, with amplitude ranging between −600 mV and −400 mV, are observed in the Permian sandstone (Figure 2). The anomaly on the top of the Sur-Frêtes ridge is enclosed on its southern part by the contact with the dolomite formations. The SP profile between the GS and the GI points has been repeatedly measured in October 95 and June 97. The electric potential difference between the two dates does not exceed 50 mV. This negative anomaly thus remained stable during this period.

[14] We performed Schlumberger resistivity measurements in the northern part of the negative SP anomaly located near the GE point (Figure 4). The ground apparent resistivity

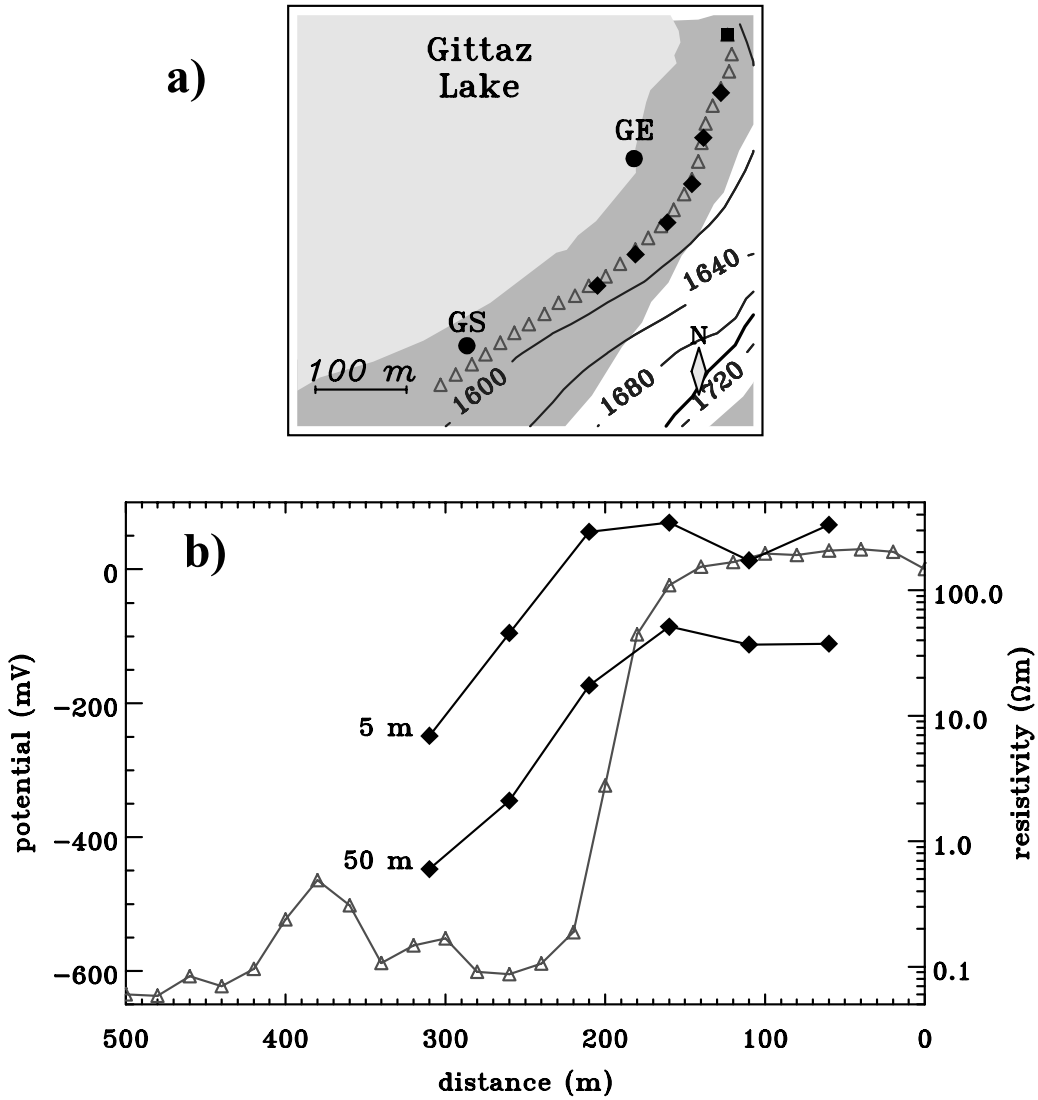

Figure 4. (a) Location of the Schlumberger resistivity sounding points (diamonds) and the SP profiling points (triangles) on the south-eastern part of the La Gittaz lake. The reference point of these SP measurements is indicated by a square. (b) Apparent resistivity and SP results. Two configurations of the Schlumberger array have been used: AB = 20 m, MN = 2 m and AB = 200 m, MN = 20 m., corresponding to sounding depths of 5 and 50 m, respectively.

has been determined for two different configurations (AB = 200 m, MN = 20 m and AB = 20 m, MN = 2 m), corresponding to sounding depths of 5 and 50 m, respectively. The apparent electrical resistivity is found to be one order of magnitude greater at 5 m depth than at 50 m depth. Outside the SP anomaly, it ranges from 200 to 400 Ω m at 5 m depth and from 30 to 50 Ω m at 50 m depth. Within 100 m, it is decreasing by about one order of magnitude, whereas the SP is decreasing from 0 to −600 mV.

[15] A static negative SP anomaly of −600 mV, associated with a resistivity decrease of more than one order of magnitude inside a metamorphic complex, has been related to the presence of graphite deposits [*Stoll et al.*, 1995]. Oxydo-reduction processes acting at the mineral-electrolyte interface were proposed to explain the SP anomaly. In a similar way, the measured high electrical conductivity, which reflects the presence of a large fraction of conductive phase, may be provided by graphite layers embedded in the coal-bearing sandstone. So the observed large negative SP anomalies may result from electrochemical processes associated with such graphite layers aligned along the geological axis. A similar anomaly is also observed in the Swiss Alps in the same formation [*Gex*, 1982].

2.3. Continuous Electric Potential Monitoring

[16] The SP monitoring array is composed of 14 measurement points (Figure 1), arranged into 20 dipoles listed in Table 1. On surface, electrodes are installed in holes (Figure 5a) filled with salted clay and soil (see appendix A for technical details). In water (points RO and GI), the electrodes rest on the lake bottom, attached to a bag filled with stones [*Trique*, 1999].

[17] Each measurement point contains as many electrodes as dipoles connected to it. This set-up allows some control

Table 1. List of the 20 Dipoles of the Electric Potential Array of the Sur-Frêtes Experiment[a]

Dipole	Potential Difference	Length, m
LLS	GI_1-RO_1	2052
LLD	GI_2-RO_2	2052
LLD′	GI_2-RO_2	2052
BBW	GS_1-LA_1	1354
BBE	GE_1-CH_1	1572
LGB	GE_2-GI_3	462
BBG	GE_3-GS_2	268
LRB	CH_2-RO_3	699
BBR	CH_3-LA_2	225
BRC	BC_1-CH_4	1077
BGC	GE_4-BC_2	543
EWN	EE_1-VN_1	757
EWS	BC_3-EO_1	760
CNW	BA_1-BC_4	51
CNE	EE_2-BC_5	114
DIW	VN_2-EO_2	137
vew	RB_1-EO_3	52
vns	VN_3-RB_2	135
VEW	RH_1-EO_4	169
VNS	VN_4-ET_1	242

[a]From *Trique* [1999]. The dipoles are composed of second-generation Pb/$PbCl_2$/kaolinite Petiau electrodes [*Clerc et al.*, 1998; *Petiau*, 2000]. The LLD and LLD′ dipoles correspond to the same dipole connected to two different electronic channels.

of electrode stability. For example, the combination RCLL = LLS − LRB − BBE + LGB = $(V_{GI1} - V_{RO1}) - (V_{CH2} - V_{RO3}) - (V_{GE1} - V_{CH1}) + (V_{GE2} - V_{GI3})$ cancels all real electrical signals but combines the drift artifacts of the eight independent electrodes forming the four dipoles.

[18] All the electrical dipoles are connected to a measuring station located on the top of the Sur-Frêtes ridge. The potential differences are read by a high input-impedance amplifier (input impedance larger than 200 MΩ) and filtered with a corner period of 30 s. The magnetic field is recorded with one three components fluxgate magnetometer installed at 50 cm deep on the top of the ridge, also filtered with a corner period of 30 s. The potential differences and the three components of the magnetic field are digitized at a frequency of 0.1 Hz and 1-min averages are stored. A meteorological station is also installed on the top of the Sur-Frêtes ridge (Figure 1), and records, with a sampling rate of 5 min: barometric pressure, air and soil temperature, air and soil humidity, rainfall, snow cover thickness, sunshine as well as direction and speed of wind. All the data from the ridge are transmitted automatically to the Bruyères-le-Châtel laboratory (located near Paris) every day by a radio-phone link.

[19] In this paper, we present the SP variations recorded by the continuous electric potential array from October 1995 to December 1998. Loss of data from March to October 1996 was caused by cable damage and in December 1997 by data acquisition problems. In December 1998, one large avalanche destroyed all aerial cables and the experiment was terminated.

2.4. Auxiliary Measurements of the Electric Potential

[20] In order to investigate the spatial variability of the electrical response reported by *Perrier et al.* [1998], we set-up in June 1998 two temporary electric potential arrays in the vicinity of two points (CH and GE) where SP variations were observed to be related to the lake-level variations (Figure 6). One measurement point of each temporary array is located at a few tens of centimeters from a point of the continuous electrical array. This set up allows the auxiliary measurements to be referred to the potential of the BC point. Each measurement point consists of a plastic tube filled with salted clay (Figure 5b) and its electric potential is sampled with a travelling electrode (Appendix A).

[21] The electric potential differences between the points of the temporary arrays are measured at different dates. Four sets of measurements were available for the temporary array on the Roselend side, and three sets of measurements were performed on the La Gittaz side, over a period of 5 months.

3. Results From the Permanent and Temporary Arrays

3.1. Short-Term Magnetic Field and Electric Potential Variations

[22] Typical variations of the recorded magnetic and electric fields are displayed in Figure 7. During a magnetic disturbance, electric signals are clearly dominated by magneto-telluric (MT) induction. These electrical signals are coherent, even for perpendicular directions, such as CNE

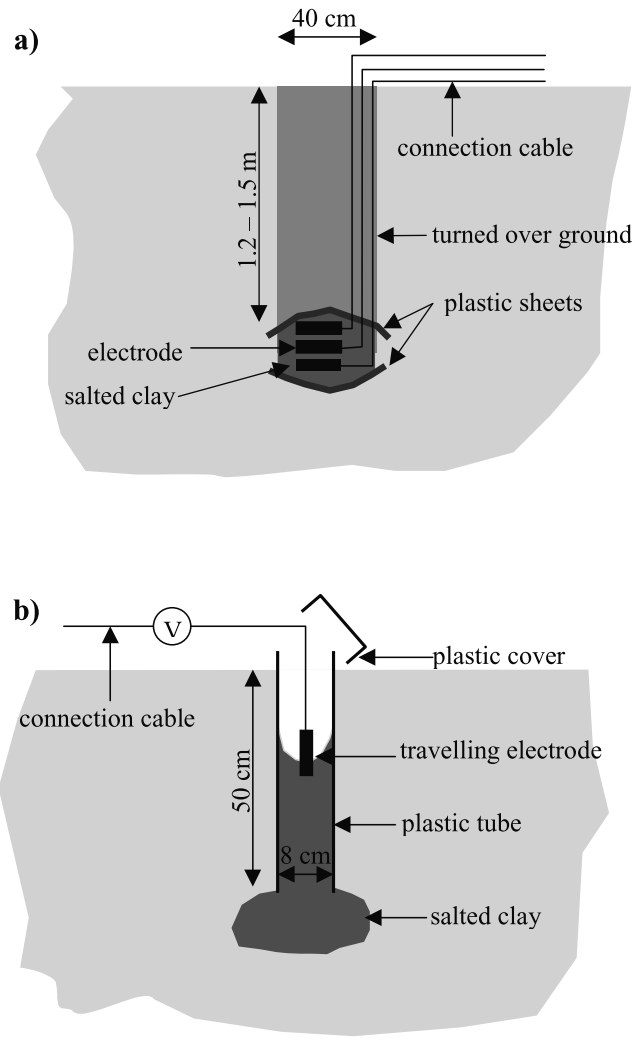

Figure 5. Sketch of the set-up used for permanent SP monitoring (a) and temporary SP arrays (b).

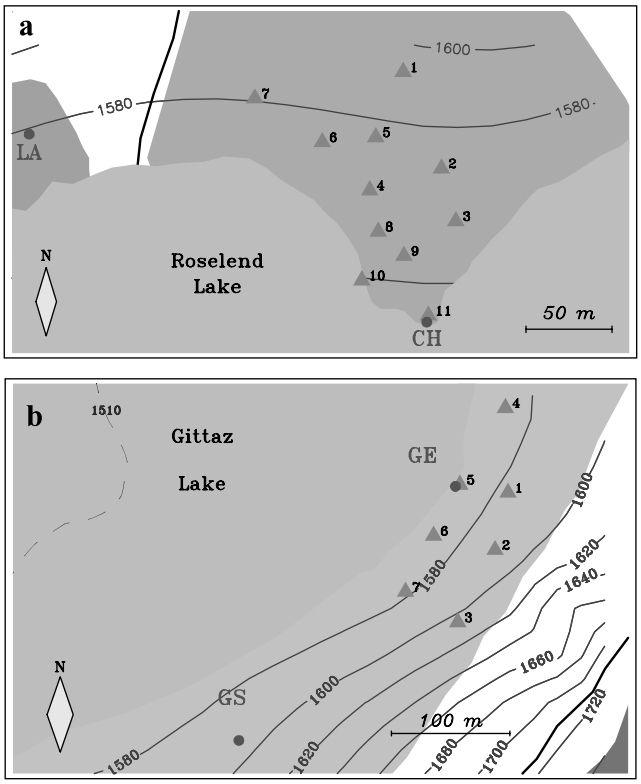

Figure 6. Layout of the temporary electric potential arrays on the Roselend (a) and La Gittaz side (b). One point of each temporary array is located near a point of the permanent array, so that all SP measurements can be referred to the BC reference point on the Sur-Frêtes ridge (Figure 1). See color version of this figure at back of this issue.

and DIW, with a strong heterogeneity in the amplitude response. Indeed, amplitudes range from a few mV/km (BBW dipole) to 1000 mV/km (CNE), with no clear relationship to the dipole length. The correlation between magnetic and electric signals is maintained for diurnal variations, which indicates a high quality of the electrical measurements. No anomalous diurnal variations, known to occur in other places [e.g., *Perrier and Morat*, 2000], are observed. This may be due to the fact that the snow cover and the meteorological conditions maintain constant soil conditions at the depth of electrodes during the whole year.

[23] In the power spectrum of the vertical component of the magnetic field, calculated with a 800 days long period, the diurnal component and its harmonics are clearly observed (Figure 8a). The component at 12.42 hours corresponds to the M_2 tidal modulation of the magnetic field [*Egbert et al.*, 1992]. These main components are also present in the power spectrum of one 800 days long data segment of the VNS dipole (Figure 8b) and confirm that electrical signals in the frequency range between 1 min and 1 day are mainly dominated by the magnetotelluric response to external magnetic field variations.

[24] The amplitude of induced electrical signals is controlled by the shallow resistivity structure, which tends to deflect the currents lines in a direction perpendicular to the main conductivity contrasts [e.g., *Le Mouël and Menvielle*, 1982; *Menvielle and Tarits*, 1986; *Zhdanov and Keller*, 1994]. The strong heterogeneity of the electric field amplitudes therefore reflects the complexity of the conductivity structure and the presence of distortion. Electric field amplification may also result from the anisotropy of the crack network [*Bahr*, 2000]. In a first approximation, one can assume that the distortion modifies the amplitude of the signals by a frequency-independent factor referred to as static-shift [*Jones*, 1988]. This seems to be the case on the Sur-Frêtes site.

[25] Furthermore, the electrical signals are strongly polarized along one axis, as illustrated in Figure 9. The direction of the horizontal polarization of the electric field, estimated using 13 couples of dipoles, varies from N80° to N140°. The mean horizontal polarization (N116°) is perpendicular to the N20° main geological axis. This indicates that the main structural contacts act as strong resistivity contrasts channeling the electrical currents. In the following, electrical signals are filtered with a loss-pass filter at 2 days and the long-term variations of SP are presented.

3.2. Long-Term Electric Potential Variations

[26] Figure 10 displays the SP variations recorded as a function of time for the three following dipoles: the 543 m-long BGC dipole, the 1.1 km-long dipole BRC and the 1.6 km-long BBE dipole (Table 1). The linear combination RTNS, defined as RTNS = BGC + BRC − BBE = $(V_{GE4} - V_{BC2}) + (V_{BC1} - V_{CH4}) - (V_{GE1} - V_{CH1})$, contains the sum of the electrical drifts of the six electrodes of the BGC, BRC, and BBE dipoles. From the beginning of the experiment until March 1998, RTNS was stable within better than 5 mV. During this period, the variations of the BRC and BBE dipoles have a similar amplitude of about 180 mV, whereas the BGC dipole displays variations with an amplitude of 30 mV. Because these variations have much larger amplitude than RTNS, it can be considered unambiguously that these variations are genuine electrical signals and not electrode drift artifacts.

[27] From March to December 1998, however, RTNS displays anomalous variations with an amplitude of about 60 mV. These variations have the same pattern and amplitude as the electric potential variations of the BBE dipole. Hence, it can be concluded that the variations of this dipole during this period are mainly produced by the drift noise of at least one of the two electrodes (GE1 and CH1) of this dipole (Table 1).

[28] The relationship between the variations of the BBE and BRC dipoles and the Roselend lake-level variations, identified in a preliminary study [*Perrier et al.*, 1998], is confirmed here by one additional year of data (Figure 10). The electric potential of the CH point, common to the BBE and BRC dipoles, is definitely controlled by the level of the Roselend lake, in a reproducible manner (Figure 11). The slope of the electric potential of the CH point to the Roselend lake level, which amounts to 2.4 mV m^{-1} of water on average, is increasing with rising lake level (Figure 11). It ranges from 2.0 mV m^{-1} of water for lake level ranging between 1507 and 1535 m, to 5.4 mV m^{-1} of water for Roselend lake level larger than 1535 m. Below a critical level of about 1507 m [*Perrier et al.*, 1998], the electrical potential can be considered independent of lake level, suggesting a saturation of the electrical source. In order to propose a model for these observations, several additional

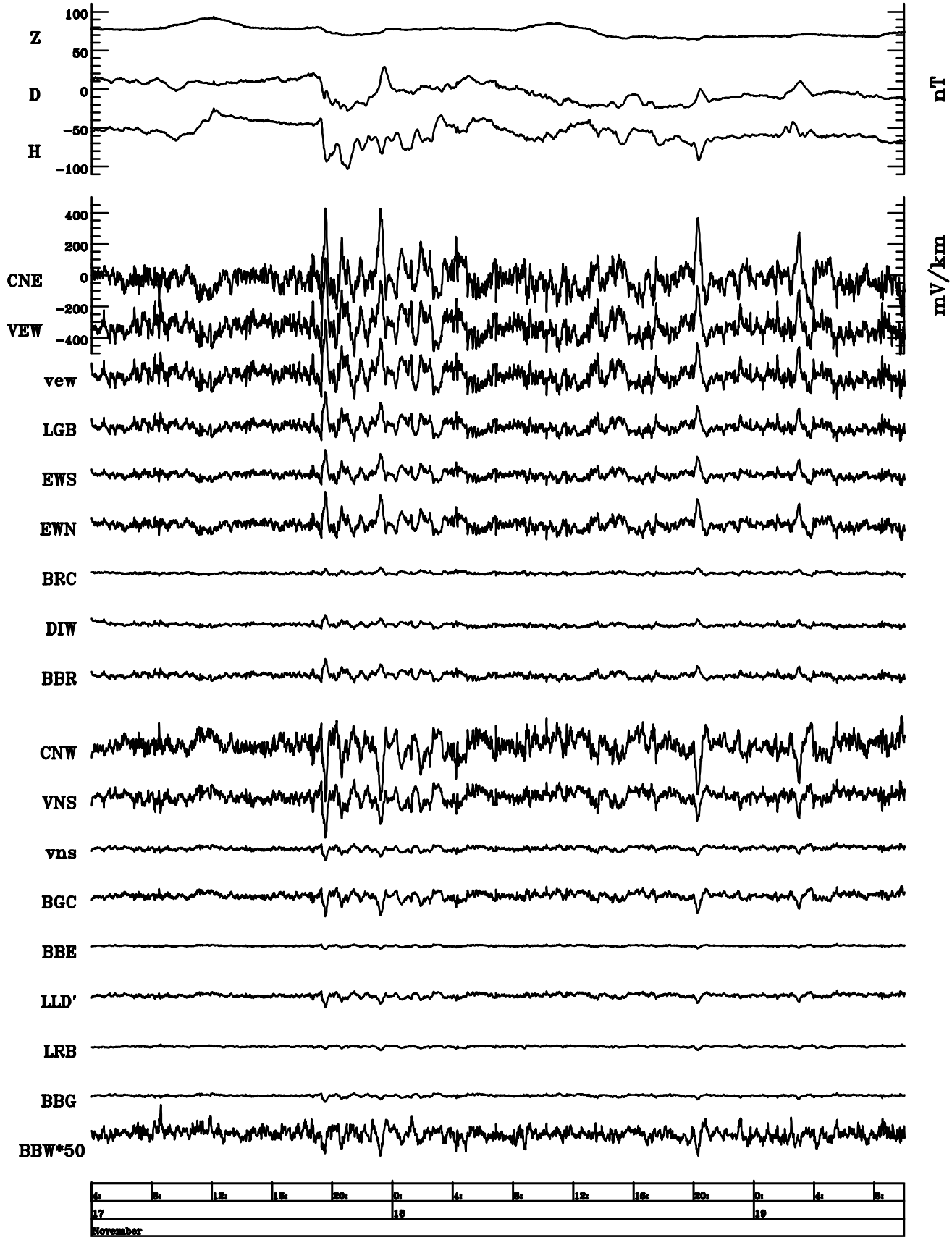

Figure 7. Variations of the three components of the magnetic field and the signals recorded on the dipoles of the permanent array, expressed in electric field units of mV/km.

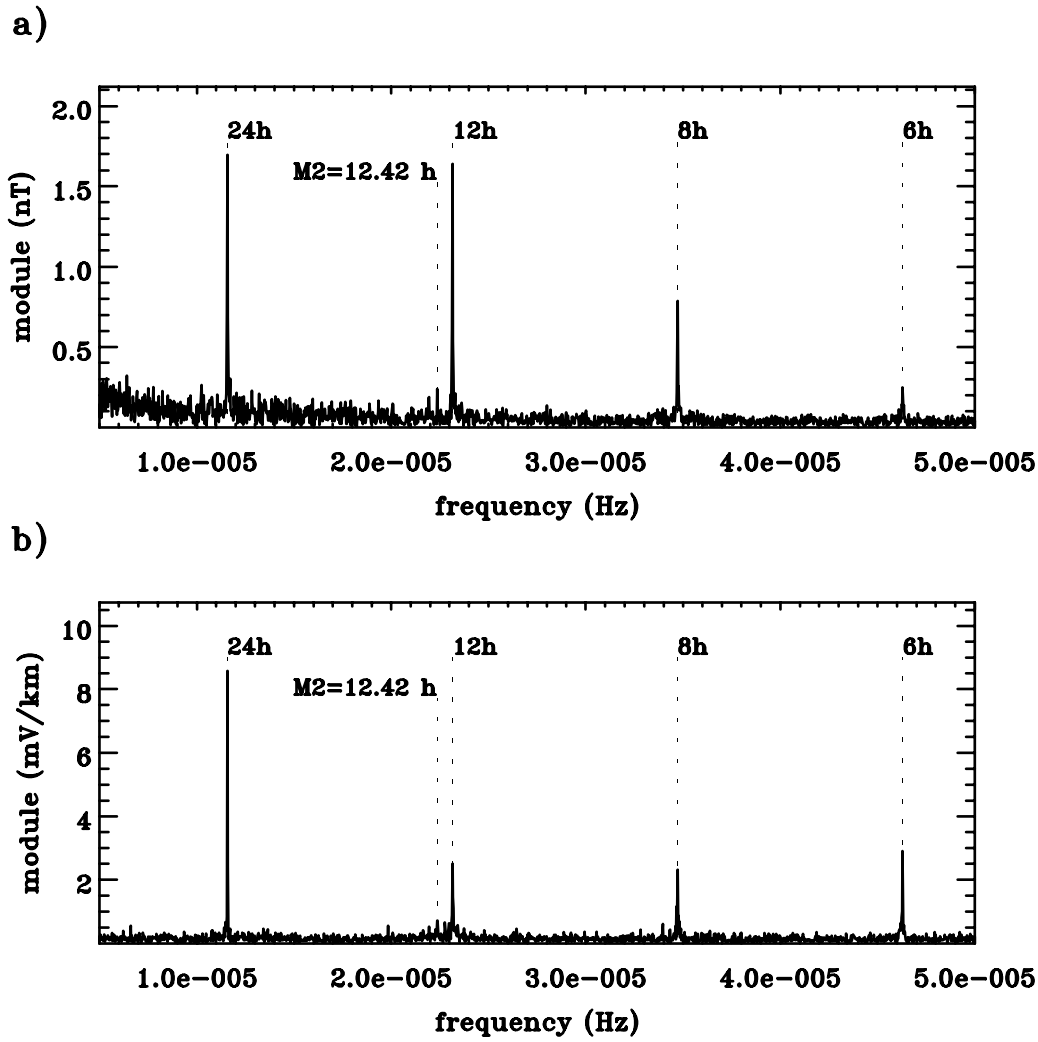

Figure 8. Amplitude spectrum of a 800 days long data segment for the vertical magnetic field (a) and the electric field recorded with the VNS dipole (b) of the permanent array (Figure 1).

pieces of information have to be taken into account, both from the permanent and temporary arrays.

[29] With this larger set of data, electric potential variations of smaller amplitude related to lake-level variations can also be observed on other points of the permanent electric potential array. Figure 12 displays the electric potential variations of the LA and CH points as well as the RO point located on the bank and in water at the bottom of the Roselend lake, respectively, taking the BC point as reference. The amplitudes of the SP variations at the LA and RO points amount, respectively, to 70 and 25 mV. The SP at the LA point (Figure 11) correlates linearly to the Roselend lake level with a slope of 0.83 mV m^{-1} of water, which is smaller than the magnitude observed at the CH point. In contrast with the CH and LA points, the slope of the SP at the RO point with respect to Roselend lake level is negative (Figure 11), with a value of -0.52 mV m^{-1} of water (Figure 11). The slope differences of the CH, LA and RO points between two years does not exceed 40%. The effect of the lake-level variations on the SP variations of the CH, LA, and RO points is therefore reproduced from year to year.

[30] Meteorological data are also plotted in Figure 12 for comparison, and illustrate the strong difference in the meteorological forcing between the period from November to May on the one hand (snow cover), and the period from June to October on the other hand (no snow). When the site is covered by snow, the soil temperature at a depth of 30 cm is stable to better than 0.1°C, whereas variations as large as 15°C can be observed otherwise. These extremely different soil conditions between the two periods do not affect the relationship between SP variations and the lake level. In addition, periods of rainfall or transient snowmelting do not induce electrical signals. The observed SP variations can therefore be considered to be due to the lake-level variations only, with little seasonal meteorological coupling.

[31] Similar observations are made at the points of the La Gittaz lake (Figure 1). The SP variations of the GE, GS and GI points with respect to the potential of the BC point, are presented in Figure 13 together with La Gittaz lake-level variations and meteorological parameters. The electric potential of the GS and GE point displays variations with an amplitude of about 30 mV. The reliability of these signals can be assessed only during the periods when the variations of RCBB are smaller than 5 mV (Figure 13). The electric potential of the GE point is clearly related to the level of the La Gittaz lake, with a slope of 0.51 mV m^{-1} of water

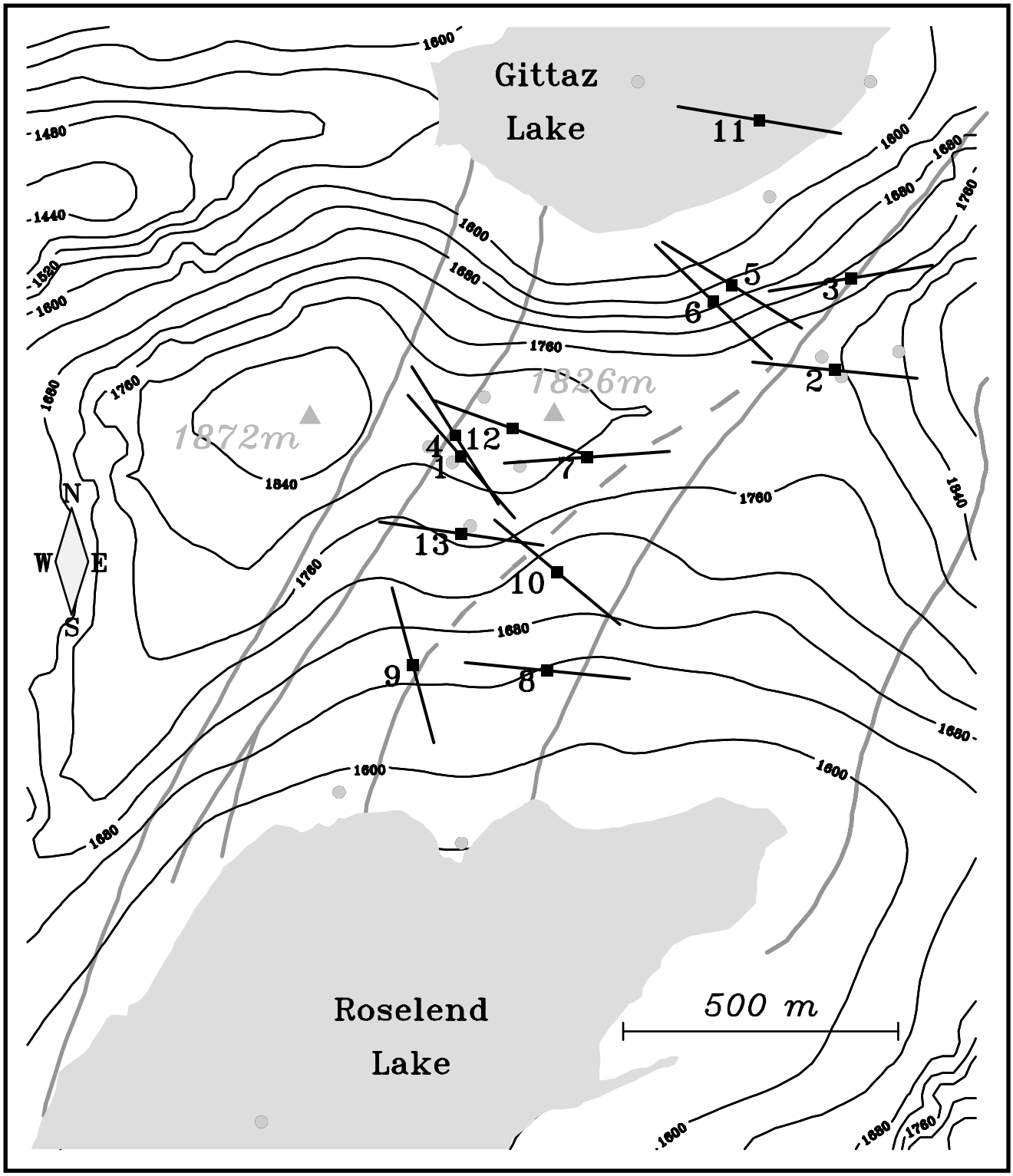

Figure 9. Polarization angle (black segments) of the electric field measured by the Sur-Frêtes electric potential array. The numbers indicate the couple of dipoles used for the estimation of the polarization angle (1 = VNS/VEW, 2 = CNW/CNE, 3 = BGC/CNE, 4 = vns/vew, 5 = BGC/EWN, 6 = BGC/EWS, 7 = BBE/EWS, 8 = BRC/BBR, 9 = LLD′/BBR, 10 = BBE/BBR, 11 = BBG/LGB, 12 = LLD′/LGB, 13 = LLD′/EWN). The center of the segments (black square) is defined as the center of gravity of the 4 electric measurement points for each couple of dipoles. The measurement points of the continuous electric potential are indicated by gray circles.

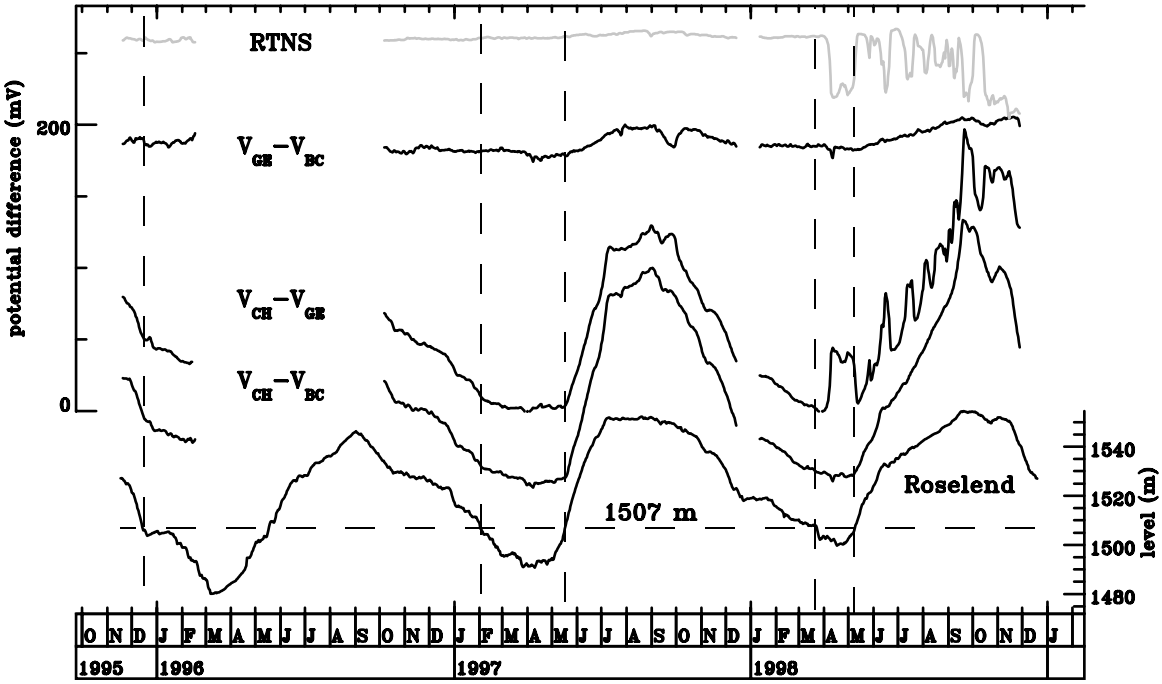

Figure 10. Roselend lake level and the potential differences $V_{CH} - V_{BC}$, $V_{CH} - V_{GE}$, and $V_{GE} - V_{BC}$ as a function of time. The RTNS signal refers to the following combination of dipoles: $(V_{CH} - V_{BC}) - (V_{CH} - V_{GE}) - (V_{GE} - V_{BC})$. The horizontal dashed line indicates the critical Roselend lake level below which the response of the electric potential $V_{CH} - V_{BC}$, $V_{CH} - V_{GE}$ to the Roselend lake level is strongly reduced.

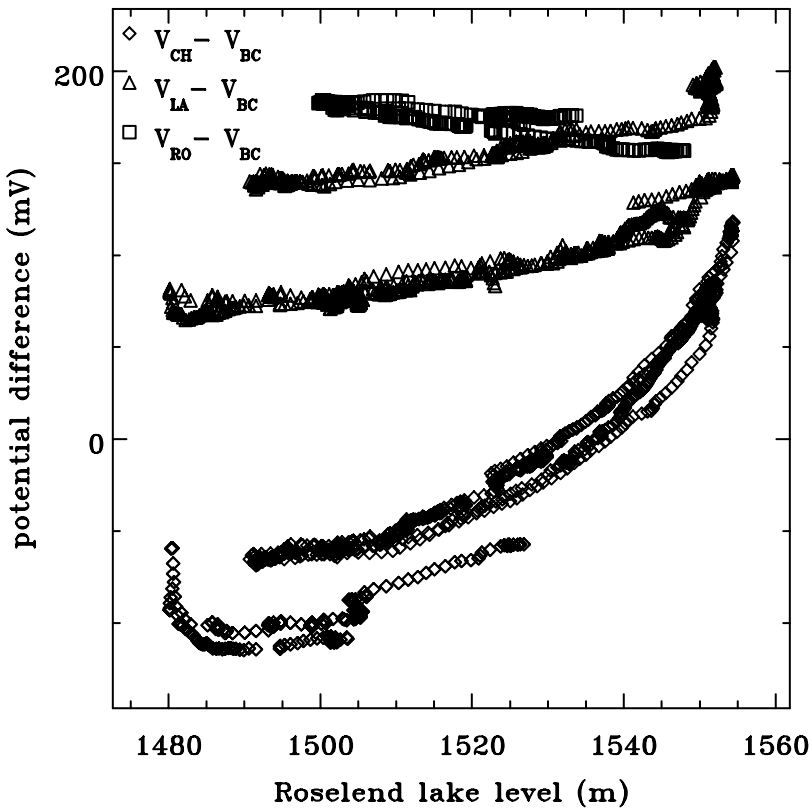

Figure 11. SP variations at the CH, LA and RO points versus the Roselend lake level. The potential at the BC point is taken as reference (Figure 1).

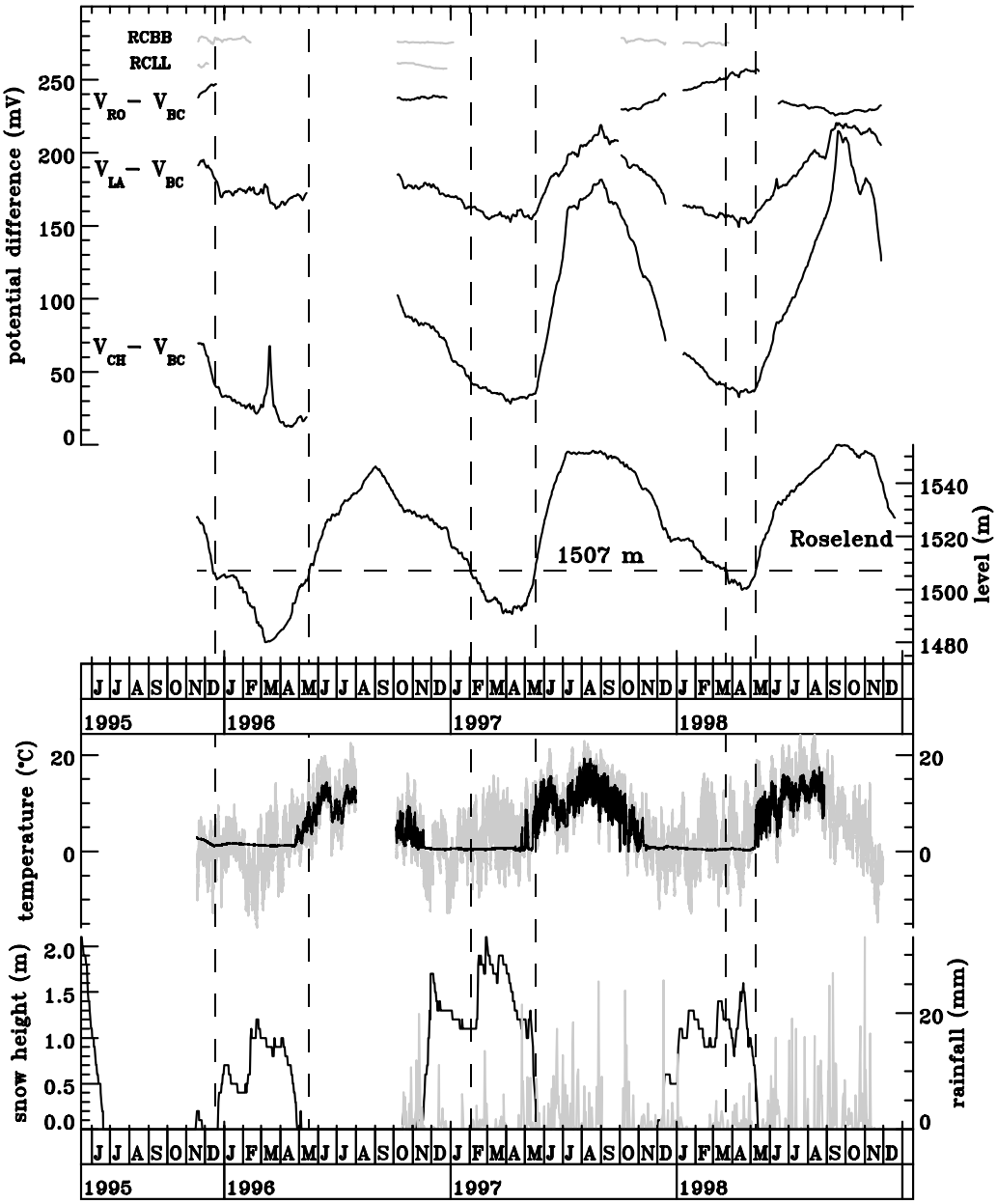

Figure 12. Roselend lake level and potential differences $V_{CH} - V_{BC}$, $V_{LA} - V_{BC}$, and $V_{RO} - V_{BC}$ as a function of time. The electric potential of the LA and RO points are obtained, respectively, from the following dipole combinations: $V_{LA} - V_{BC} = -BBR - BRC$ and $V_{RO} - V_{BC} = -LRB - BRC$. RCBB refers to the combination BBE − BBW − BBG + BBR and RCLL to the combination LLS + LGB − BBE − LRB. On the bottom, the air and soil temperature (at 30 cm depth), the snow thickness, as well as the rainfall are displayed as a function of time.

(Figure 14). A new phenomenon is however observed: when the level of the La Gittaz lake level is above 1556 m, the slope at the GE point changes sign (Figure 14), with a slope of -2.9 mV m^{-1} from August to September 1997, and -1.4 mV m^{-1} from August to September 1998. The GI point, which presents variations of the order of 70 mV, exhibits a negative correlation to the La Gittaz lake level (Figure 14), with a slope of -1.42 mV m^{-1} of water. When the lake level is below the critical elevation of 1529 m, no relationship between the electric potential of the GI or the GE point and the La Gittaz lake level is observed, in support of a saturation or threshold mechanism which is more conspicuous in the case of La Gittaz than Roselend lake. For lake level below 1556 m, the response at the points GI and GE is reproducible within 30% from year to year. As previously for the Roselend data, the seasonal potential variations do not appear to bear any direct relationship to the meteorological cycle (Figure 13).

[32] The main characteristics of the observed SP variations related to the level variations of the Roselend (Figure 12) and La Gittaz lakes (Figure 14) are similar. The response of the SP variation with respect to lake-level variation is positive for points located on the bank of the lakes, and negative for points located on the bottom of the

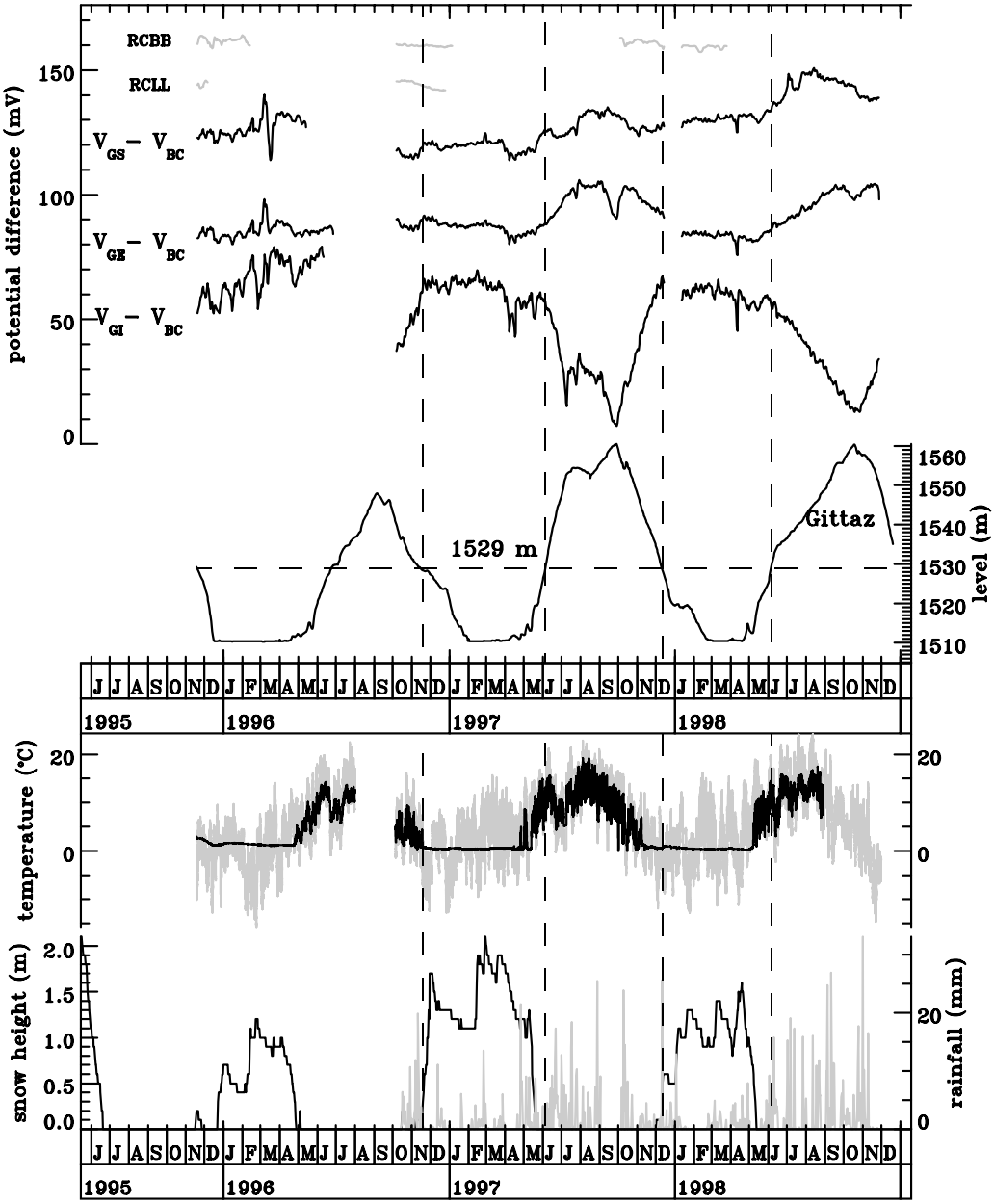

Figure 13. La Gittaz lake level and potential differences $V_{GS} - V_{BC}$, $V_{GE} - V_{BC}$, $V_{GI} - V_{BC}$. The SP of the GS and GI points with respect to BC are obtained from the linear combinations $V_{GS} - V_{BC} = -BBG + BGC$ and $V_{GI} - V_{BC} = -LGB + BGC$, respectively. RCBB refers to the combination BBE − BBW − BBG + BBR and RCLL to the combination LLS + LGB − BBE − LRB. On the bottom, the air and soil temperature at 30 cm, the snow thickness, as well as the rainfall are displayed as a function of time.

lakes. The slope is reproducible from year to year, but differs from point to point, with values ranging from 0.7 to 4.2 mV m^{-1}. The eight points of the permanent array located on the Sur-Frêtes ridge (BC, BA, EE, VN, EO, RB, ET and RH, see Figure 1) do not display clear seasonal SP variations related to the lake-level variations.

3.3. Electric Potential Variations From the Temporary Arrays

[33] Results obtained from the temporary electric potential arrays are presented in Figures 15 and 16. On the bank of the Roselend lake, the amplitude of the spatial variations of the electric potential amounts to 370 mV (Figure 15a). A coherent increase of the potential with time, for increasing lake level, is observed on average for all points. We focus our attention on the electric potential difference measured between lake level values of 1532 and 1554 m, which corresponds to the maximal SP variation induced by a lake level change measured during the observation time. All the points display a positive electric potential increase for the lake level increase of 22 m (Figure 15b). The measured amplitude ranges between 28 mV for the point 1 located at the elevation of 1610 m and 126 mV for the point 11 located near the CH point at the elevation of 1555 m.

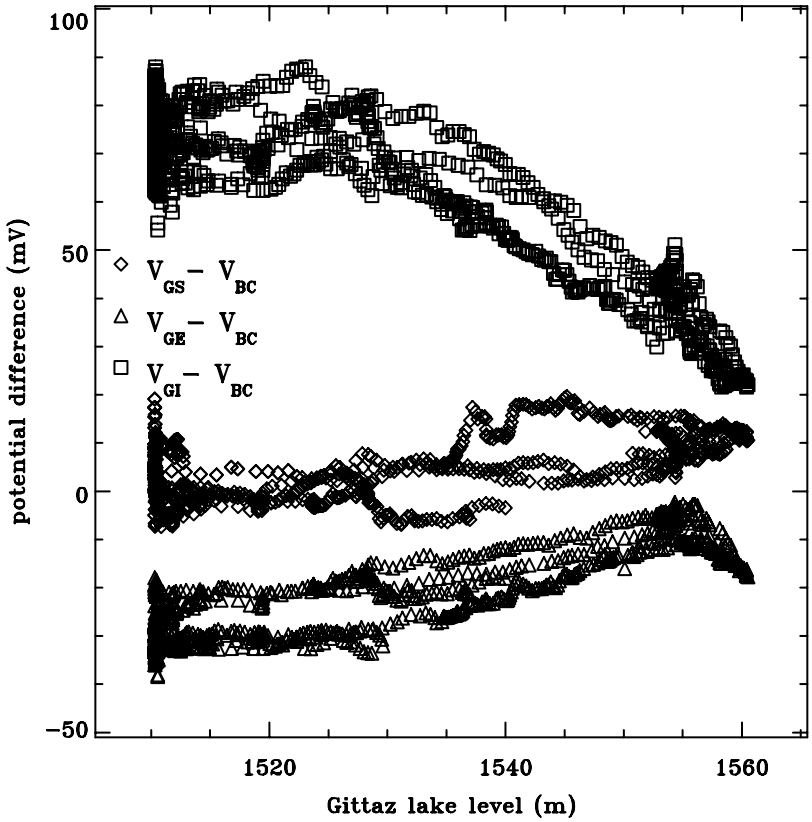

Figure 14. SP variations at the GS, GE and GI points versus the Roselend lake level. The potential at the BC point is taken as reference (Figure 1).

[34] Similar effects are observed on the bank of the La Gittaz lake (Figure 16). The amplitude of the spatial SP variations amounts to 360 mV. For a La Gittaz lake level increase of 19 m, an increase of the electric potential with amplitude ranging between 10 and 25 mV has been measured for points 1 to 6, whereas a decrease of the electric potential of −23 mV has been observed at point 7.

[35] The auxiliary measurements, totally independently from the permanent array, therefore confirm, on the bank of the lakes, a positive response of SP with respect to the lake level. In addition, these temporary arrays indicate that the SP temporal variations depend on the position at a scale of about 30 m. The electric potential varies more with lake level for points closer to the lake (Figure 15), and this is an important constraint for the interpretation.

3.4. Static Shift Seasonal Variations

[36] Relative MT amplitude variations between two electrical dipoles can be used to monitor resistivity changes at a depth of the order of the dipole length [e.g., *Park and Fitterman*, 1990; *Park*, 1991, 1997]. As mentioned before, the Sur-Frêtes ridge is characterized by a distortion of the MT signals causing all dipoles to be proportional to each other in a first approximation. Static shift changes associated with local changes in the conductivity structure could then be observed by comparing the relative intensity of the MT signals as a function of time.

[37] In the following, amplitude ratios between electric dipoles are calculated for each day using periods from 10 min to 4 hours. A robust procedure is used, eliminating portions of the signals producing non-Gaussian tails in the amplitude distribution. Most of the ratios that can be constructed with the Sur-Frêtes permanent array (Figure 1) display seasonal variations. A detailed discussion of these effects is beyond the scope of this paper. Here we only present the ratios LGB/VNS and CNW/CNE, which display seasonal variations that can be interpreted qualitatively.

[38] These two pairs of dipoles are particularly illustrative because their short-term signals are highly correlated. Indeed, the CNW/CNE and the LGB/VNS ratios can be determined with a precision of 0.5% and 1.2%, respectively. Therefore, time variations of the order of 6% and 18%, respectively, more than 10 times larger than the determination error, can be observed unambiguously (Figure 17). The time variations of the LGB/VNS ratio (Figure 17a) follow the variations of the La Gittaz lake. Such time variations could be due to the change of telluric current distortion induced by the change of the water volume in the lake, which has a resistivity of about 50 Ω m.

[39] The case is different for the time variations of the CNW/CNE ratio in Figure 17b. These variations are clearly associated with the Roselend lake level but with a definite time lag, which amounts to about 30 days, observed for example at the minimum end of April 1996 or beginning of May 1997. Such variations can not be attributed to the conductive mass of the lake water itself, but point to the existence of changes in the conductivity structure of the ridge with a characteristic time of about 30 days. This can

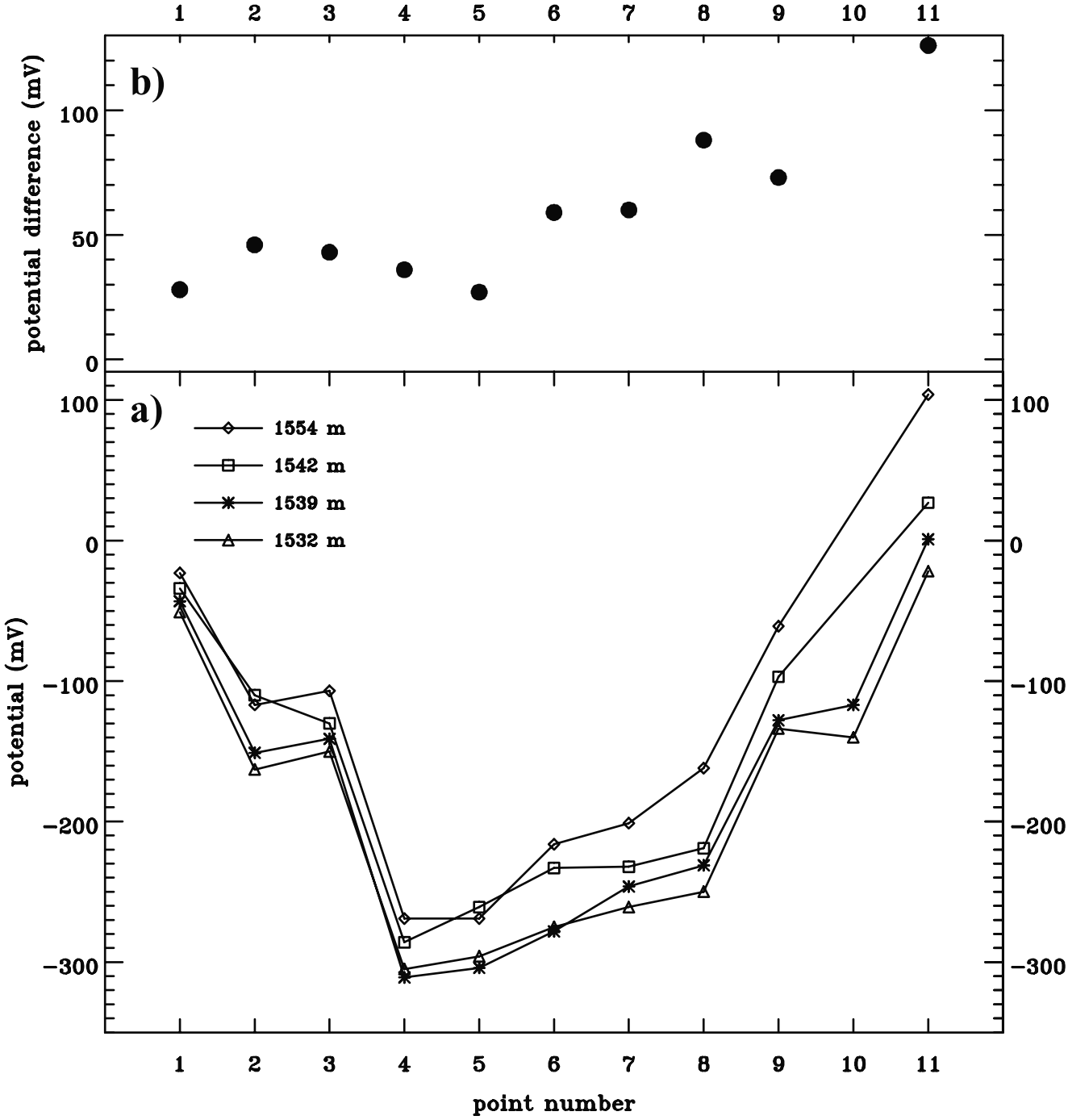

Figure 15. (a) Electric potential measurements performed on the temporary electric potential array located on the bank of the Roselend lake for different values of the Roselend lake level h_R. The measurements are referred to the potential of the BC point. Only two measurements were performed at the point 10. Indeed the point 10 was under water for the Roselend lake level of 1554 m. It has not been retrieved under the 1 m thick snow cover of the Roselend lake level at 1542 m. The measurements have been performed on 18 June 1998 (h_R = 1532 m), 17 July 1998 (h_R = 1539 m), 21 September 1998 (h_R = 1554 m), and 26 November 1998 (h_R = 1542 m). (b) Electric potential difference related to the maximal lake level increase from 1532 m to 1554 m.

be interpreted qualitatively as a direct evidence of fluid circulation inside the ridge.

[40] Such a surprisingly high sensitivity of the MT amplitudes to resistivity changes is probably not true in general. No seasonal variations of the static shift was for example observed in a dedicated experiment in Garchy [*Clerc et al.*, 1998]. The effect observed in Figure 17, in addition to the large forcing, probably results from the

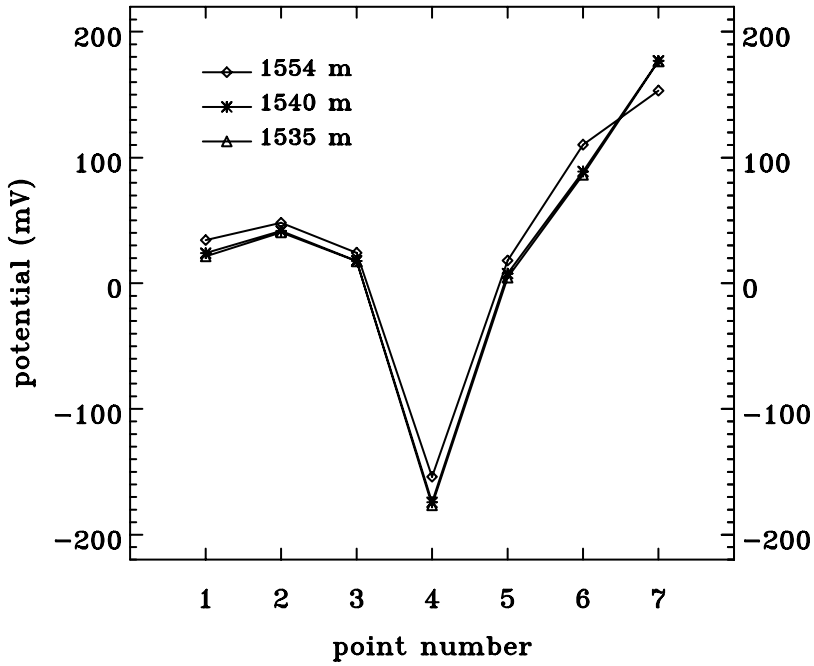

Figure 16. Electric potential measurements from the temporary SP array located on the bank of the La Gittaz lake for different values of its level h_G. The measurements are referred to the potential of the BC point. The measurements have been performed on 18 June 1999 (h_G = 1535 m), 17 July 1998 (h_G = 1540 m), and 16 September 1998 (h_G = 1554 m).

complex 3D structure of the MT induction fields in the heterogeneous contact zone of the site, where shallow distortions may be locally amplified.

4. Discussion and Interpretation

[41] In the following, we discuss how the observations can be interpreted in terms of streaming potentials. First, it is necessary to investigate whether apparent electric potential variations can result from the modulation of constant current sources by the changes of the amount of conductive water in the lakes. Indeed, the water of the lake tends to form a quasi-equipotential volume, which averages the electric potential at the bedrock on the lake banks.

4.1. Modulation of Electrical Source of Constant Intensity by Lake-Level Variations

[42] Let us assume the presence of electric current source with constant amplitude. The negative static SP anomalies observed at the site indeed suggest the existence of large zones where oxydo-reduction processes take place, which may act as embedded current sources with constant amplitude. We used a numerical calculation to test this hypothesis, using point current sources in various positions of a 2D profile of the ridge, and for each position the electric potential is calculated at various points of the ridge representing locations of our SP monitoring array [*Trique*, 1999].

[43] For remote sources located about 500 m at least from the lakes, the results indicate that SP variations can indeed be observed when the lake level is varied. However, these SP variations concern the ridge as a whole, and in particular, seasonal variations larger than about 15 mV should have been observed using the dipoles located on the top of the ridge. For positions of the sources leading to negligible signals on the ridge, the negative response for points in the lake cannot be accounted for. Consequently, a remote electrical source locally modulated by resistivity variations associated with the lake level changes produces qualitative features incompatible by the data.

[44] For sources located less than 100 m away from the lake banks, the situation is different. Negligible effects can be produced on top of the ridge and the electric potential can change in opposite directions above and below water level when the lake level is increasing. However, for acceptable configurations of the sources, the variation of SP is strongly nonlinear with a maximum slope for water level at the altitude of the source. These features are not observed with the field measurements. Therefore, the hypothesis of the modulation by lake-level variations of the SP associated with a constant local electrical source can also be reasonably rejected.

4.2. Models With Time-Varying Electrokinetic Sources

[45] We now examine models with a local electrokinetic source which a time-dependent amplitude, controlled by the lake level. We consider a very simple geometry for this source, namely a porous cylinder, in which fluid flow induces electrical currents. The cylinder, which is located in a medium with homogeneous conductivity, can be approximated by a dipolar electrical source [*Bernard*, 1992]. For realistic geological conditions of *pH* and electrolyte concentration, the electric potential should increase with decreasing piezometric head along the percolation path [*Jouniaux and Pozzi*, 1995a, 1995b; *Lorne et al.*, 1999a; *Revil et al.*, 1999b], hence producing a positive electrical source at the exit of the column and a negative source at its high pressure end.

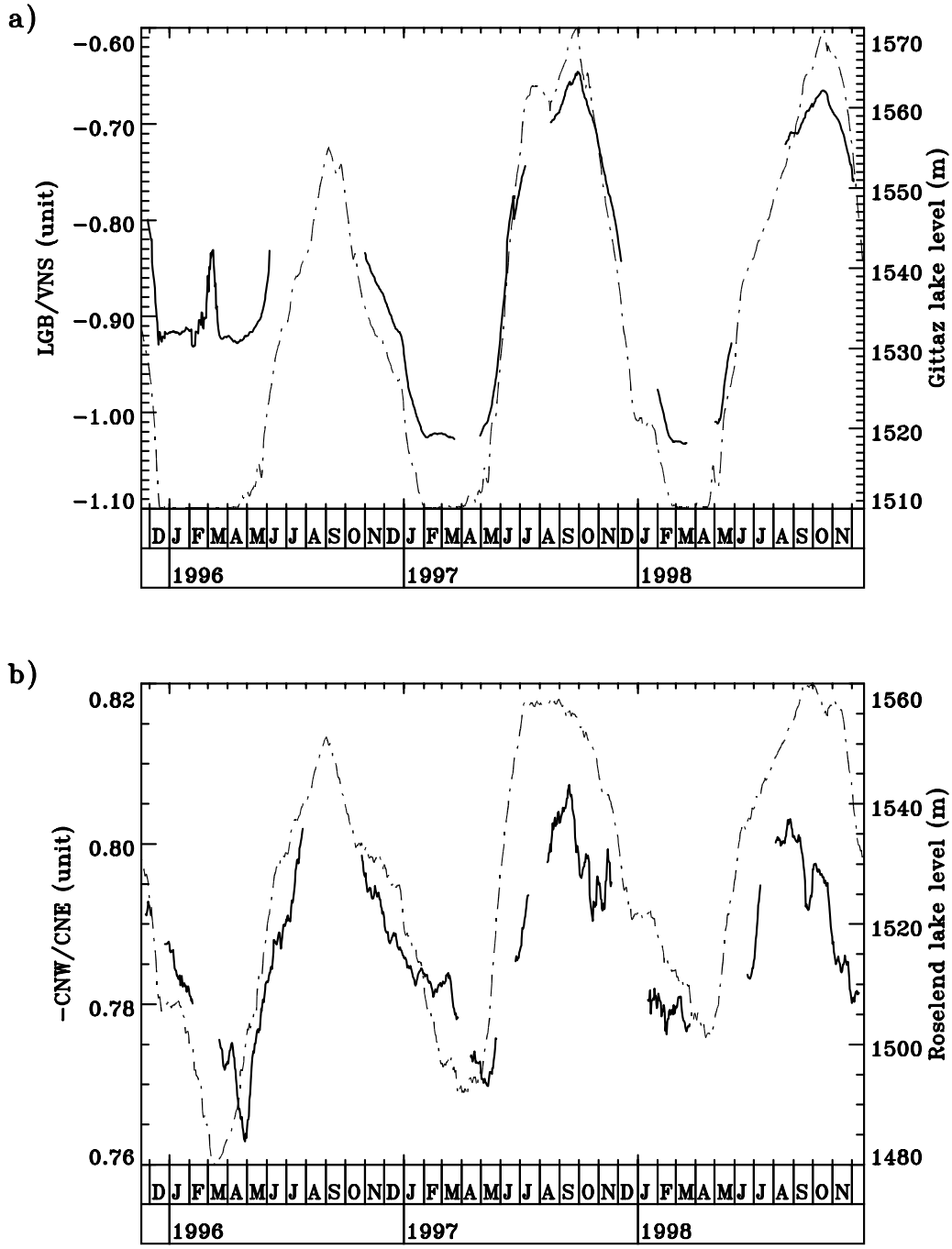

Figure 17. Electric field amplitude ratios LGB/VNS (a) and CNW/CNE (b) as a function of time.

[46] The water is supposed to flow from one fluid reservoir inside the lake bank to the reservoir lake through the porous cylinder. Therefore, the intensity of the resulting electrokinetic source is controlled by the lake level. Neglecting current leakage, the electric potential drop can be expressed as $\Delta V = C_s \rho g \Delta h$, where C_s is the streaming potential coefficient (SPC) of the percolated rocks, ρ is the water density, g is the gravity and Δh is the level difference between the inlet of the zone of fluid flow and the lake level. Ignoring surface conductivity effects, the SPC can be expressed as: $C_s = -\varepsilon_f \zeta/(\eta_f \sigma_f)$, where ζ is the electric potential at the mineral-water interface, ε_f, η_f and σ_f are the dielectric constant, dynamical viscosity and conductivity of the fluid, respectively [*Mizutani et al.*, 1976; *Lorne et al.*, 1999a; *Revil et al.*, 1999b].

[47] We suppose that the elevation of the inlet is constant and the bottom of the circulation zone has the elevation of the lake surface. The amplitude of the fluid pressure gradient in the percolation zone is increasing with decreasing lake level (Figure 18a), hence the intensity of the electrokinetic source. If the fluid flow is nearly horizontal (Figure 18a), then the electric potential near the bank is controlled by the intensity of the positive source and is increasing when the lake level is decreasing, which is the

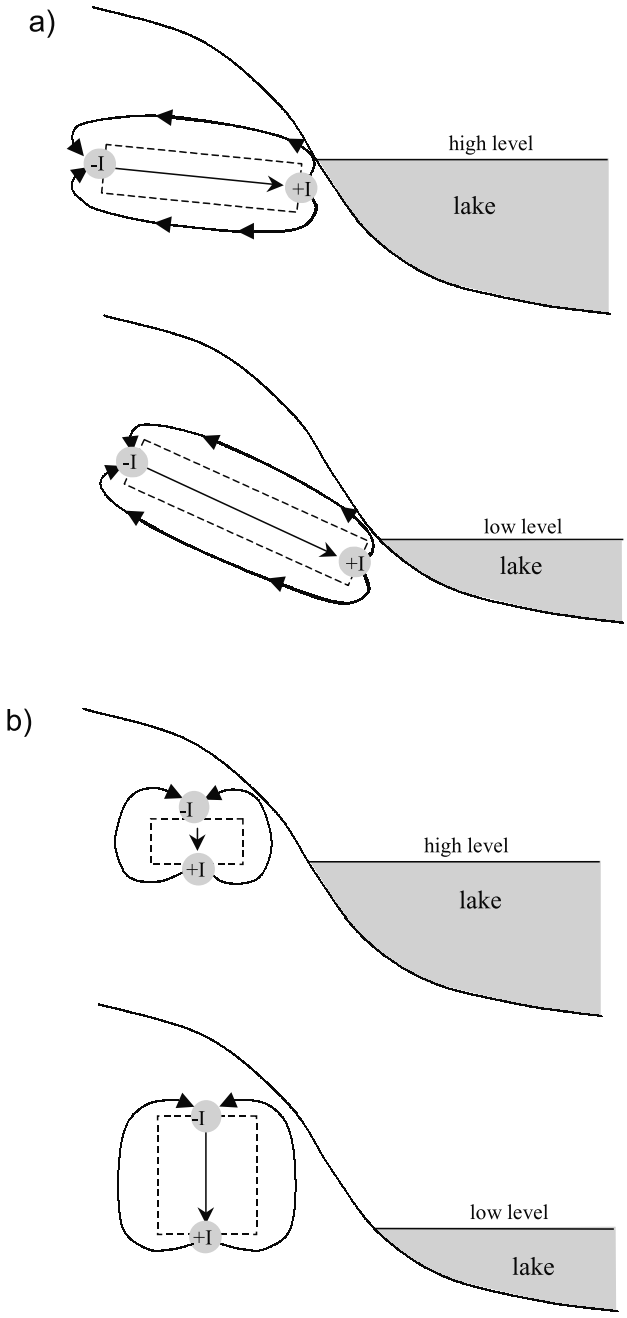

Figure 18. Sketch of horizontal (a) and vertical (b) groundwater flow with their associated electrical current distributions.

opposite of what is observed. This geometry thus can not account for the observations.

[48] Let us consider instead a vertical orientation of the percolation area (Figure 18b) [*Perrier et al.*, 1998]. The electric potential near the bank is then controlled by the negative pole of the column, and is then decreasing when the lake level is decreasing. Such a geometry may therefore account for the positive slope of the electric potential with respect to the lake level observed at points CH, LA and GE, which would then be located near the top of the percolation zone. The RO and GI points in contrast would be located near the bottom of the percolation system in order to explain the negative SP response observed at these points.

[49] In Figure 18b, the size of the percolation zone increases with decreasing lake level. The varying elevation of the bottom of the percolation zone may thus add a non linear component to the relationship between the electric potential and the lake level for fixed points located on the bottom of the lake, which could explain the relationship between SP and level at point CH (Figure 12). The observed linear relationship between the electric potential and the lake level for points RO and GI suggests however a fixed size of the percolation zone.

[50] A percolation zone of fixed size implies that the outlet has a constant elevation. If the lake level is lower than the elevation of the outlet, the piezometric gradient in the percolation zone is then maximal and does not depend anymore on the lake level. The intensity of the EKE source is then saturated. This would account for the behaviors observed at point CH and more clearly at point GI (Figures 12 and 14). Consequently, EKE induced by a vertical percolation zone for water controlled by the lake level, provides an explanation for the observed pattern of the electric potential variations. In this model, groundwater flows from a zone of constant pore pressure, e.g., a perched fluid reservoir, to an outlet located on the bottom of the lake.

[51] There is no direct evidence of fluid flow near the banks of the lakes which could help support our model. The constant pressure for percolating water may be provided by perched aquifers located inside the banks of the lake. However, perched aquifers have not been directly evidenced in the coal-bearing and calcareous sandstone units. A perched aquifer has been observed in the cellular dolomite unit located close to the CH point. One fractured zone with continuous water drainage has been evidenced near the La Gittaz dam structure in the crystalline basement [*Electricité De France*, 1951], but this does not guaranty the existence of groundwater flow inside geological structures nearby the two lakes.

[52] No time delay greater than two days is observed between the electric potential variations and the lake level changes. This information provides an order of magnitude of the lower limit of the permeability of the percolation zone in the proposed model. According to a porosity of the medium of 10^{-2} and a characteristic length scale of the percolation system of about 50 m, the permeability of the percolation zone must be greater than 10^{-16} m^2. This value is coherent with the values of the rock permeability measured in situ on the site, which do not exceed 10^{-15} m^2 [*Electricité De France*, 1951].

[53] As mentioned before, fluid circulation in the Sur-Frêtes ridge is suggested by the seasonal variations of static shift with time lag as long as 30 days. Such large scale groundwater circulation in the ridge suggests the possibility of circulation on much shorter spatial and timescales as well, especially in the immediate vicinity of the lakes, and permeability values in the 10^{-15} to 10^{-16} m^2 range could be assumed reasonably. Such fluid circulation with a response faster than 2 days may have an effect on the seasonal variations of static shift, but such variations can not be interpreted unambiguously in this case. The best evidence

for groundwater flow near the lake banks remains the time variations of SP themselves.

[54] This model of vertical groundwater circulation near the lakes therefore seems reasonable in first approximation, but we need to investigate whether, in this framework, first the observed spatial variation and second the absolute amplitude of the SP variations can actually be accounted for.

4.3. Interpretation of the Spatial Variations of the SP Variations

[55] The slope of the electric potential with respect to the lake level measured on the temporary electrical array varies from point to point (Figure 15), with a clear dependence as a function of altitude as illustrated in Figures 15 and 16, and in Figure 19. This dependence can be accounted for in the framework of the previous EKE model. Indeed, lake-level variations not only change the amplitude of the electrokinetic source, but also change the distribution of electric currents.

[56] In order to estimate in a simple manner the effect of the geometrical attenuation of the electric potential for the proposed electrokinetic source, we calculate the potential distribution generated by a dipolar source, with an amplitude modulated by the lake level, using a 3D code [*Spitzer*, 1995]. For practical reasons, we use a resistivity model restricted to the bank of the Roselend lake (Figure 19). The elevation of the line crossing the CH point with a N27°E direction is chosen for the topography of our model. The model (1400 m length by 232 m height) is divided into 20 m $\times$4 m cells. A low resistivity structure (80 Ω m), representing the zone of groundwater flow, is introduced in the bedrock near the lake. The intensity I of the current sources, which is modulated by the lake level, reaches a maximal value of 4 A for a lake level value of 1504 m and 0 for a lake level value of 1560 m. The maximal intensity is chosen to fit the measured electric potential. The potential difference is then calculated at the ground surface between Roselend lake level values of 1532 and 1554 m.

[57] The calculated response of the electric potential to the lake level, which is presented as a function of the elevation of the Roselend bank in Figure 19, is in agreement with the observations. This indicates, first, that the decreasing slope with increasing topography can be attributed to the geometrical attenuation of the electric potential generated by an electrical source located in the bank of the Roselend lake. Furthermore, the lateral extension of the zone of fluid flow inside the bedrock, which contributes to the electric field, appears limited in this case, and the elevation of the top of the percolation zone must be located near the maximum level of the Roselend lake. In contrast, our preliminary model [*Perrier et al.*, 1998] proposed an extended source more than 100 m away from the maximum lake level, a view which is not supported by the measurements from the temporary array.

[58] For the bank of the La Gittaz lake, six out seven points of the temporary array show an increase of the electric potential for an increase of the lake level from 1535 to 1554 m (Figure 16). The average increase amounts to 9 mV for the points located at the elevation of 1605 m (points 1, 2, and 3) and 20 mV for the points located at the elevation of 1570 m (points 4, 5 and 6). The estimated decrease of the slope with the elevation, which amounts to 0.016 mV m^{-2}, is smaller by a factor 6 than the decrease measured for the Roselend temporary array. This factor is coherent with the ratio of the mean slope at the CH point to the mean slope measured at the GE point, which amounts to 8. The CH and GE points are both located near the highest level position of each lake. This confirms that the decreasing response with increasing elevation on the lake bank is produced by the attenuation of the electric field, whereas the difference of response measured at points CH and GE may be attributed either to a difference of the amplitude of the EKE source or to a difference in the resistivity structure between the two sites.

[59] According to the proposed electrokinetic model, the electric potential is increasing linearly with diminishing piezometric level downward along the percolation column. This pattern is shown by the electric potential profiles P1 and P2 performed on the bottom of the Roselend lake (Figure 3). However, no relationship between the electric potential and the topography on the profile P2 is observed for elevation greater than 1510 m. The presence of a static positive SP anomaly of the order of 120 mV at this place may modify the SP distribution. This explanation is supported by the static electric potential difference measured between the point 11 and the point 10 of the temporary electric potential array (Figure 15), which also amounts to 120 mV.

4.4. Interplay of Horizontal and Vertical Groundwater Flow

[60] Variants of our model with a horizontal electrokinetic source, which in its simple form was found to be incompatible with the data, can be considered. A secondary water flow could indeed take place in the unsaturated zone from the surface to the top of the unconfined aquifer [*Aubert et al.*, 1991; *Aubert and Yéné Atangana*, 1996]. Both water flow pattern may then act as coupled electrokinetic sources controlled by the lake-level variations. The water flow from the aquifer to the lake provides an horizontal electrical source, whereas the downward fluid flow in the unsaturated zone provides a vertical electrical source (Figure 20b).

[61] In such a framework, the positive correlation between the electric potential and the lake level on the bank may be explained by the vertical electrical source, whereas the negative correlation observed on the bottom of the lakes may be produced by the horizontal electrical source. Therefore, the decrease of the slope with the elevation measured on the Roselend temporary array may be explained by the dip variations of the aquifer surface below the temporary array induced by the lake-level variations.

[62] The negative slope of the electric potential to the lake level, observed at the GE point for La Gittaz lake level values greater than 1556 m (Figure 14), could be attributed to the existence of a secondary local electrokinetic source. The source has to be located near the GE point, since similar electric potential variations are not observed at the GS and GI points. This suggests the existence of an unsaturated horizon near the GE point. When the La Gittaz lake level exceeds the elevation of the unsaturated zone, the water flow from the lake to the unsaturated zone could produce a negative potential on the surface. In this way, the amplitude of the electric potential above the percolation zone should

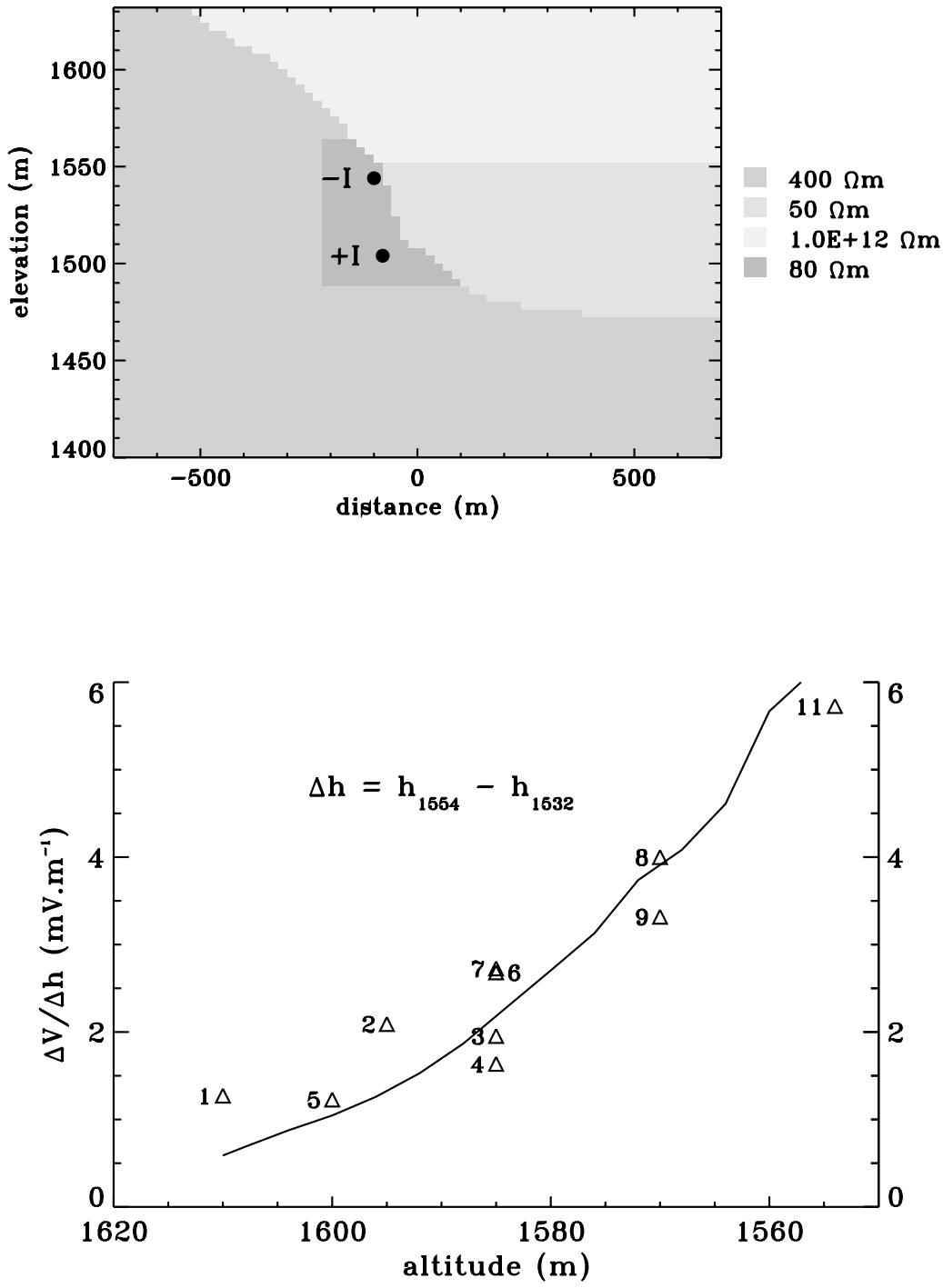

Figure 19. Response of the electric potential to the lake level as a function of the topography. (a) Resistivity model. The areas with resistivities of 10^{12}, 400, 80, and 50 Ω m represent the atmosphere, the host rocks, a fluid saturated zone, and the Roselend lake, respectively. The fluid saturated zone represents the percolation zone. The corresponding electrokinetic source is represented by a dipolar electric current source (black points). The absolute amplitude *I* of the current sources modulated by the lake level, is fixed to be maximal for the lake level of 1504 m and 0 for a lake level of 1560 m. The maximal amplitude of the current source is fixed to 4.2 A in order to fit best the electric potential measurements performed on the Roselend bank. (b) Sensitivity of the electric potential measured on the Roselend temporary array corresponding to the Roselend lake level increase from 1532 to 1554 m as a function of the elevation of the points (triangles). The calculated response on the surface of the host rocks is indicated by a dashed curve.

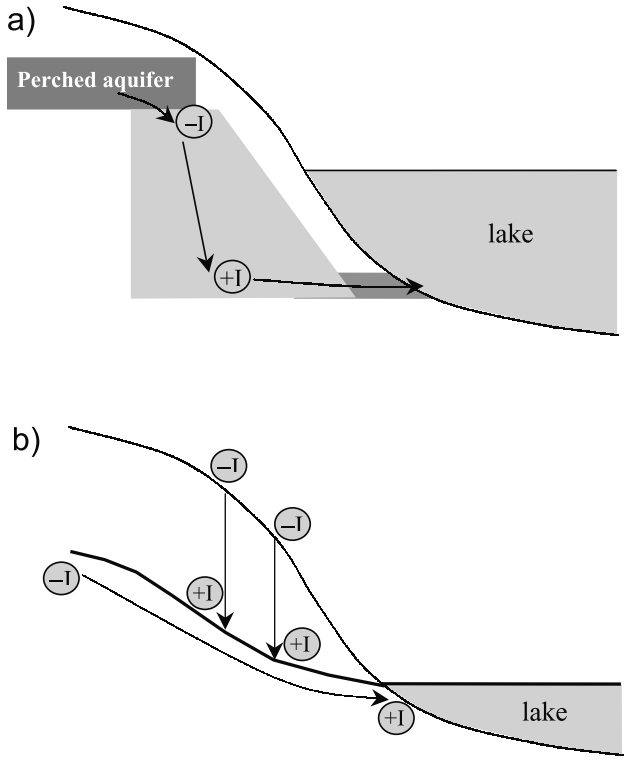

Figure 20. Two possible models for the fluid flow and electric response patterns. (a) Vertical fluid flow provided by a perched aquifer. (b) Variations of the unconfined aquifer associated with lake-level variations. The vertical arrows indicate the groundwater flow inside the unsaturated zone, whereas the others indicate the fluid flow under the surface of the unconfined aquifer.

then be related to the water height above the saturated-unsaturated transition. The slope at the GE point for lake level values greater than 1556 m has increased by a factor 2 between 1997 and 1998 (Figure 14). This fact could be explained by a change of the geometry of this particular percolation system.

[63] The proposed model is non unique, and additional refinements are needed to account for all the features of the data. Nevertheless, within a given model, such as the vertical groundwater column described in Figure 20a, it is interesting to compare the measured potential variations with some theoretical estimate, and point out the limitations in such a comparison.

4.5. Comparison of the Amplitude of SP Variations in the Field With Laboratory Measurements

[64] First-order values of the SPC can be estimated from the measured SP variations. For that purpose, the measurement points are supposed to be close to one end of the percolation system, and the leakage currents are neglected. The potential difference along the percolation column is then estimated to amount to two times the potential measured at one extremity with respect to the potential at infinity [*Perrier et al.*, 1998]. Therefore, values of the SPC extrapolated from field measurements range between 12 (RO and GE points) and 84 mV/0.1 MPa (CH point).

[65] In the following, we discuss whether these values of the SPC extrapolated from field measurements are acceptable in terms of the EKE. In order to investigate the variations of the SPC on the various geological units of the sites, and also within the same geological formation of the calcareous and coal-bearing sandstone, the EKE has been measured in laboratory on crushed rocks sampled in the corresponding geological units of the site (Figure 1). These measurements have been performed using the experimental setup described by *Lorne et al.* [1999a].

[66] Measurements on individual samples of Fontainebleau sandstone have demonstrated that the SPC does not exhibit any intrinsic dependence of the SPC with permeability for electrolyte resistivity smaller than 100 Ω m [*Lorne et al.*, 1999a, 1999b]. The resistivity of spring and lake water measured on the Sur-Frêtes site ranges between 25 and 90 Ω m with an average of about 40 Ω m [*Hautot et al.*, 2002]. Therefore, the measurements with crushed samples allow the comparison of the differences of the SPC between the sampled sites.

[67] Figure 21a displays the measured SPC as a function of the electrolyte resistivity. The corresponding SPC ranges between 14 and 50 mV/0.1 MPa (Table 2). These measured values are in agreement with the previous estimates of the SPC inferred from field measurements (12 to 84 mV/0.1 MPa). The new laboratory values are however smaller than the value of 66 mV/0.1 MPa measured for Fontainebleau sandstone [*Lorne et al.*, 1999a]. The difference compared with Fontainebleau sandstone comes from several reasons. First, the ζ potential corrected for surface conductivity [*Lorne et al.*, 1999a], presented in Figure 21b, is different for the considered rocks compared with Fontainebleau sandstone. The values of the ζ potential are in good agreement with the previous results of *Lorne et al.* [1999a] for the same rocks, except for the cellular dolomite for which a smaller value was reported by *Lorne et al.* [1999a]. The measured values of the ζ potential tends to be smaller, and do not exhibit the variation with resistivity $\rho^{0.23}$ measured for Fontainebleau sandstone [*Lorne et al.*, 1999a]. The measurements for the various samples (Figure 21b), except GHFN, indicate that the ζ potential is independent of the electrolyte resistivity or may even decrease slightly with electrolyte resistivity. In addition, the contribution of surface conductivity is larger for the considered rocks than for Fontainebleau sandstone, which tends to reduce the SPC for the same ζ potential. Applying general scaling laws or values of the ζ potential measured for other rocks can therefore lead to significant mistakes in estimating the value of the SPC.

[68] However, experimental measurements of the streaming potentials do not solve the problem of estimating the values of the coupling coefficient relevant for field scales. The fact that the measured range values agree quite well at first sight with the field measurements is indeed misleading.

[69] First of all, one noteworthy feature of the experimental measurements is the observed variation of the SPC by approximately a factor 3 between the rock samples originating from the same calcareous sandstone unit, namely the GCCH, GCRO and GCP38 samples, whereas a difference by a factor 2 is observed between the crushed rocks sampled in the coal-bearing sandstone (GRH, GHP50, and GHFN samples). This fact means that the SPC of one geological unit can not be determined from one sample

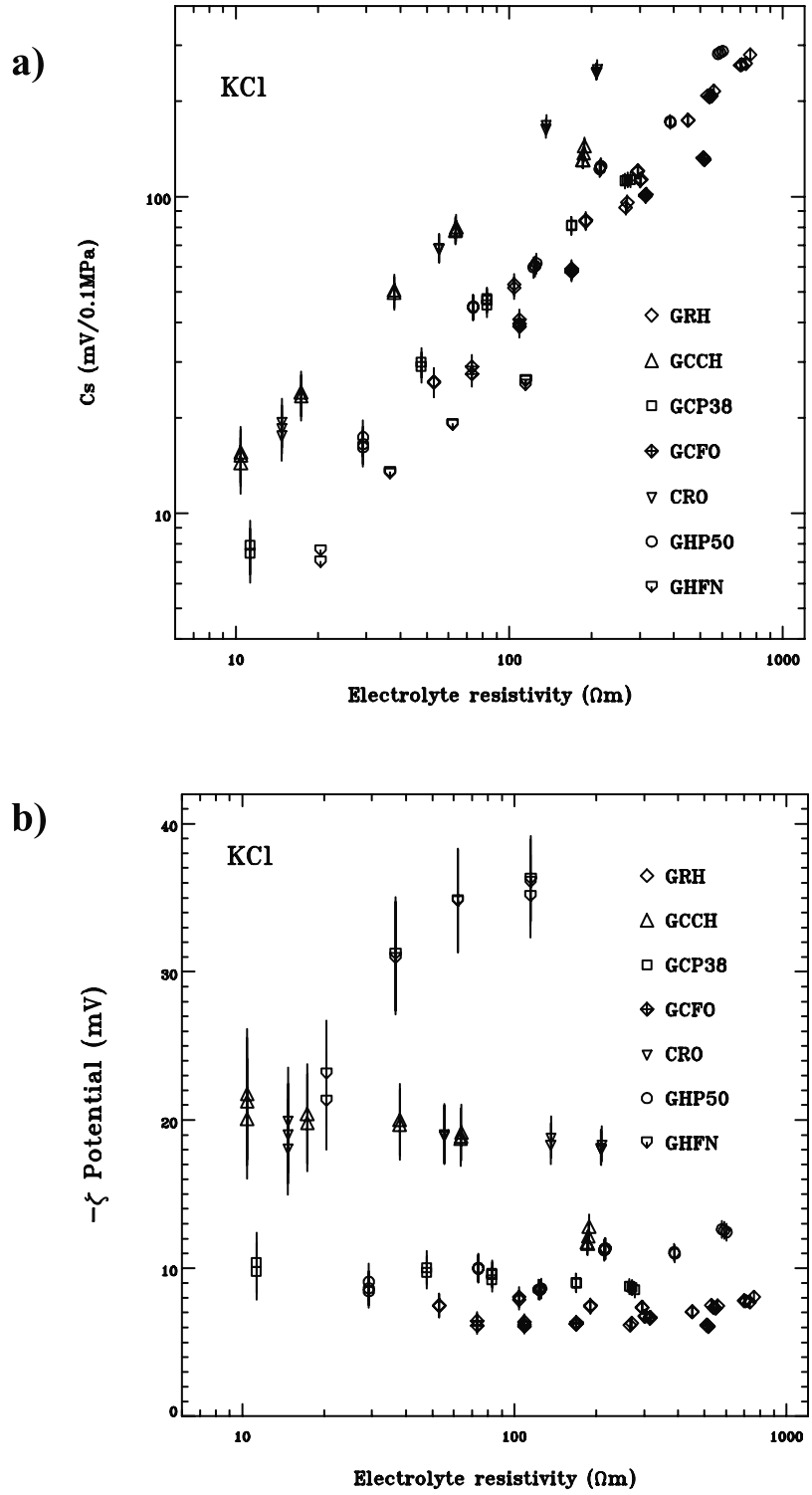

Figure 21. Streaming potential coefficient (a) and ζ potential (b) as a function of the electrolyte resistivity measured with crushed rocks sampled on the Sur-Frêtes site (see sampling locations in Figure 1).

only. Large variations may happen due to local differences in mineralogy or chemical alteration, itself resulting from water circulation. A past history of water circulation in a rock system may thus affect the electrokinetic response in a dramatic fashion.

[70] Second, there is some uncertainty on the value of the percolating water resistivity. If a value of 300 Ω m is used instead of 40 Ω m, the SPC changes from 26 to 250 mV/0.1 MPa. Larger values of the electrolyte resistivity can not realistically be considered but, in some formations with low carbonate content (GCP38 and GRO), the resistivity value of an electrolyte in chemical equilibrium with the rock can be larger than 1000 Ω m (Table 2). In such formations, rain or snowmelting water would travel without increasing much

Table 2. Laboratory Measurements of the ζ Potential and the Streaming Potential Coefficient Performed on Crushed Rocks Sampled[a]

Sample	−ζ, mV	C_s, mV/0.1 MPa at 40 Ω m	C_s, mV/0.1 MPa at 300 Ω m	Equilibrium, ρ_{eq}, Ω m	C_s (ρ_{eq}), mV/0.1 MPa
GCRO	18.5 ± 0.5	50	255	1200	5100
GRH	7.3 ± 0.1	20	265	460	170
GCCH	13.5 ± 0.4	53	145	60	74
GCP38	9.0 ± 0.2	25	113	3000	100
GCFO	6.3 ± 0.1	17	131	460	125
GHP50	10.7 ± 0.2	23	53	210	120
GHFN	32.4 ± 0.8	14	26	210	70

[a]See Figure 1. Samples were obtained from the cellular dolomite unit (GCRO), the calcareous sandstone unit (GCCH, GCFO, and GCP38), and the coal-bearing sandstone unit (GH, GHP50, GHFN). The equilibrium resistivity is the value reached several days after the rock sample has been in contact with pure dionized degassed water.

their salt content, with streaming coefficients as large as 5000 mV/0.1 MPa for GCRO.

[71] Finally, the assumption of negligible leakage currents for estimating the coupling indicated by the field results can be questioned. This problem needs to be considered in the context of the full coupled electric current and flow problem.

4.6. Estimating the Effect of Coupling Between Source and Leakage Currents

[72] Variations of the apparent resistivity structure of the medium are produced by the variations of the lake levels, as evidenced by the observed static shift variations (Figure 17). As illustrated before (Figure 19), modifications of the apparent resistivity produced by the lake-level variations may modulate the electric potential distribution produced by the electrokinetic source. Additional effects can result from the coupling of electrical and groundwater flow.

[73] The influence of the leakage currents can be qualitatively evaluated using the analytical model developed by *Adler et al.* [1999]. In this model, a vertical fractured column is considered in two dimensions and is characterized by SPC C_{sf}, rock resistivity ρ_f, and permeability k_f. This column, where flow is imposed by the boundary conditions, is imbedded in a porous medium characterized by C_{sp}, ρ_p, k_p. Calculated values of the maximum anomaly are given in Table 3 for values of the parameters relevant for the present study. The width of the column is 100 m for a 100 m height. Case 1 illustrates the effect of leakage currents when $C_{sf} > C_{sp}$. The effect is rather small, of the order of 20%. In Case 2, $C_{sf} = C_{sp}$. In this case, the potential is independent of the medium resistivity. This fact can be actually be checked analytically. One can rely on this property when, on average, the coupling coefficients are equal on various geological units; the effect of leakage currents on the potential can then be deemed as negligible. However, when $C_{sf} < C_{sp}$ (case 3), the electric potential can be reduced by a factor 2 to 3, depending on the resistivity of the porous medium. In this case, note that the amplitude of the anomaly is increased when the resistivity of the surrounding medium is decreased. This reduction is not affected much when the amount of flow leakage in the surrounding medium is increased (k_p increased, Case 4). Note that the situation with $C_{sf} < C_{sp}$ could be happening on our site, as GCRO is measured to have the largest SPC, although the real SPC around the observation points is unknown.

[74] To summarize, the effect of leakage currents, which is important only if the SPC of the surrounding medium is larger than the SPC of the percolating fluid column, leads to variations of the same order of magnitude than the relative differences of the SPC values measured on the various geological units, as well as the relative differences of the

Table 3. Estimation of the Influence of the Leakage Currents on the Magnitude of the Electric Potential Anomaly on the Surface[a]

Case	C_{sf}, mV/bar	k_f, 10^{-12} m^2	ρ_f, Ω m	C_{sp}, mV/bar	k_p, 10^{-12} m^2	ρ_p, Ω m	Maximum Surface Anomaly, mV
Case 1	50	10	100	10	0.1	10	−187
						100	−211
						1000	−238
Case 2	50	10	100	50	0.1	10	−244
						100	−244
						1000	−244
Case 3	10	10	100	50	0.1	10	−208
						100	−137
						1000	−64
Case 4	10	10	100	50	1	10	−190
						100	−125
						1000	−59

[a]A 100 m × 100 m model has been chosen. It is composed of one fractured medium, in which fluid flow is driven by gravity, embedded in one porous medium. The fractured (f indices) and porous (p indices) media are characterized by their SPC, permeability, and fluid resistivity. The maximum surface anomaly is then calculated using the analytical model developed by *Adler et al.* [1999].

SPC values on the same geological unit. This intrinsic uncertainty implies that an accurate modeling of the electrokinetic response in a natural system appears to be a difficult task. The only robust conclusion that can be drawn at this stage is that the values of the SPC measured in the laboratory account for the first order of magnitude of the observed effects measured in the field, which supports the interpretation in terms of electrokinetic effects.

[75] The spatial variability of the conductivity structure is involved in the variations of the slope of the electric potential to the lake level. As shown before (Figure 19), the presence of a conductive zone contributes to the attenuation of the electric field generated by an electrokinetic source in the vicinity of the measurement point. On the La Gittaz side, the lack of response at the GS point does not imply that the electrokinetic source is located far from the GS point. Indeed, since the GS point is located near a high conductive zone (Figures 2 and 6), the electric field generated by an electrokinetic source close to it may be strongly attenuated because of leakage currents and therefore may not be detectable at this point.

[76] Furthermore, the potential difference measured at point 7 of the temporary array of the La Gittaz side is negative and amounts to −23 mV. Point 7 is located near a high conductive zone (Figure 6). The mobile charge carriers may then produce a local electrical induced polarization in the electric field generated by the electrokinetic source. The sign of the induced electric field should then be opposite to the main field. This could explain the local inversion of the slope of the electric potential to the lake level, which still has to be confirmed by further measurements.

4.7. Static SP Anomalies Versus Dynamical Pattern of SP

[77] The main negative anomalies have been measured in the coal-bearing sandstone unit (Figures 1 and 2), and an electrochemical explanation is likely in this case, as mentioned before. The static pattern of the electric potential has to be studied in relation with the geology, to eliminate anomalies which are not related to the groundwater flow. In our experiment, there is no straightforward relationship emerging between the SP distribution, and the SP time variations associated with lake-level variations. More than the static SP, it is more the associated conductivity structure of the formation that can affect locally the electrokinetic response to fluid flow. In the case of the coal-bearing formation, a static SP of −600 mV is observed in association with a high conductivity (Figure 4), which will cause the EKE induced SP variations nearby to be attenuated.

[78] The area enclosing the CH and LA points and the Roselend temporary electric potential array, is characterized by a negative anomaly of the order of −100 mV (Figure 2). The electrokinetic signature of one shallow downward groundwater flow is a negative anomaly. This anomaly could be located above the percolation zone. However, no clear relationship appears between these static negative anomaly and the amplitude of the coupling coefficient relating the electric potential to the lake level. Therefore, the discrimination of this negative anomaly as the electrical signature of downward vertical fluid flow can not be ascertained in this case. The additional measurements with the temporary arrays indicate that no clear association can be made between the observed static SP and the structure causing the time variations. This association was one assumption in our preliminary model [*Perrier et al.*, 1998] that this more detailed study does not confirm.

5. Conclusion: SP and Groundwater Flow

[79] Several conclusions can be drawn from this experiment on the possible characterization and monitoring of fluid flow through electric potential measurements. In this paper, electric potential measurements show unambiguous seasonal variations related to lake-level variations. They provide evidence that fluid flow occurs inside the bedrock, and that electric potential variations are produced by an electrokinetic mechanism.

[80] The continuous electrical array used in this experiment gives a satisfactory long-term stability, thus demonstrating the technical feasibility of such set-ups at kilometer size systems, and illustrating the detection power of this technique. In addition, we show that temporary electrical arrays, periodically measured, can also be used to identify long term variations of the electric potential. Although the time resolution is relatively poor, such arrays are easy to implement and can provide measurement error of the order of one mV. They can be used to extract spatial information of the dynamical features of SP and they are therefore complementary to a permanent array, which can monitor reasonably only a limited number of points.

[81] Furthermore, as already demonstrated in Parkfield, electrical arrays can monitor indirectly the shallow resistivity of the medium through the amplitude of the induced electrical signals (static shift). In the present experiment, seasonal variations associated with changes in the groundwater distribution are identified, opening the way for more detailed investigations. Such effects are important to study because they can produce artifacts when trying to monitor deep electrical structures, and deserve more studies in dedicated experiments.

[82] In contrast, analysis of the static pattern of SP does not provide clear evidence of electrical signals related to fluid flow. No straightforward relationship appears between the static and the dynamical features of the electric potential in Sur-Frêtes. In the present experiment, the main static SP anomalies seem to be all redox in origin. Moreover, their amplitude is at least five times greater than the amplitude of the temporal SP variations related to fluid flow. Our experiment therefore suggests that the study of the shallow fluid circulation can not be achieved from the study of static SP measurements only. The study of the dynamical features of the electric potential distribution is essential to assess the relationship between electric potential and fluid flow. For this purpose, temporary electric potential arrays provide an efficient and cheap tool to characterize areas affected by strong electric potential variations, which are signatures of shallow fluid flow. However, additional data like hydrogeological, geological or geophysical data may shed light on the relationship between static SP pattern and fluid flow like in geothermal fields [*Revil and Pezard*, 1998; *Revil et al.*, 1999b] or volcanic areas [*Michel and Zlotnicki*, 1998, *Sasai et al.*, 2001]. Field results from very low frequency and audio magnetotelluric soundings performed on the Sur-Frêtes ridge indicate the presence of shallow groundwater

circulation, with conductive pockets from 200 to 400 m depths [*Hautot et al.*, 2002]. The relationship between the conductive structures obtained from electromagnetic imaging and groundwater flow forced by the lake level, suggested by the SP time variations, remains however to be investigated. Without additional information, there is no certainty at this stage that the conductive zones imaged by MT provide relevant clues for our interpretations in terms of the electrokinetic effect.

[83] A detailed modeling of the hydroelectrical processes occurring inside the bedrock is currently difficult to achieve on the present site and this is probably true also for most real cases. Indeed, the SPC measurements performed in laboratory on crushed rocks sampled on the field indicate that the amplitude of the SPC can vary by a factor 3 inside the same geological formation. Moreover, the extrapolation of the laboratory measurements to the field conditions need to constrain the dependence of the SPC of each rock formation on *p*H and fluid conductivity as well as the geochemical properties of the water flowing inside the geological formations. Furthermore, the electric, electrokinetic and transport properties of the rocks located near the percolation zone also have an important role in the amplitude of the local electrokinetic response to fluid flow. Although the SPC extrapolated from field measurements agree to first order with the laboratory measurements, a realistic and detailed modeling of the distribution of fluid flow and electric potential on the Sur-Frêtes site remains difficult.

[84] However, it should be pointed out that the real issue may not be the quantitative understanding of electric potential variations associated with fluid flow. Indeed, the time variations of the electric potential are themselves an unambiguous indicator of groundwater flow and in this sense a valuable monitoring tool. It is for the moment the only method through which groundwater flow can be evidenced using surface measurements. This experiment demonstrate that such electrokinetic effects can be actually identified in a kilometer-size natural system, and interpreted in terms of groundwater flow.

[85] Electric potential variations associated with water level variations observed in this experiment may have practical applications in the monitoring of artificial lakes, as first pointed out by *Ogilvy et al.* [1969]. Other applications may be considered, such as for the monitoring of the groundwater flow near large ship locks (e.g., Three Gorges project in China) or water pollution by waste disposal. The SP monitoring of fluid flow in mechanically unstable areas could also provide an additional tool to monitor the occurrence of landslides [*Bogoslovsky and Ogilvy*, 1977; *Bogoslovsky et al.*, 1977]. However, this experiment also clearly indicates that electrokinetic effects can be detected if the groundwater forcing is large enough (such as water level variations of the order of 50 m), if they occur at shallow depth (such as flow in the lake banks) and if the measurements are performed basically on the sources (such as CH or GE). Detecting groundwater flow associated with precursory stress changes thus appears to be a difficult task, especially electrical effects associated with a large nucleation area within the crust [*Bernard*, 1992], unless transient phenomena lead to an amplified local response [*Trique et al.*, 1999; Perrier et al., in preparation, 2002]. However, if monitoring arrays are designated and operated with care, SP variations as small as a few mV per month could be identified. It is therefore justified to attempt investigations aiming at surface detection of groundwater flow at a km depth, first in well controlled contexts. Operational applications might be reasonable to consider only in a later stage.

Appendix A: SP Measurement and Monitoring Techniques

A.1. SP Mapping Methods

[86] Two different methods were used to obtain the static map of the electric potential. From September to October 1995, a mobile dipole method was used: a 50 m long dipole is displaced along profiles and the electrodes are swapped between two consecutive measurements in order to reduce the instrumental drift noise of the electrodes. However, the error value was estimated to be of the order of 80 mV per kilometer of profile. In July 1997, the profiles were measured using a fixed electrode for profiles having a maximal length of 600 m. The error value was estimated to be less than 2 mV over one profile.

[87] The two electric potential profiles P1 and P2 on the bottom of the Roselend lake were performed using a fixed electrode located at about 1 m from the CH point on the lake bank, taken as reference (Figure 4). The mobile electrode was dragged on the bottom of the lake from a boat, with steps of about 50 m, on a line perpendicular to the lake bank.

A.2. Permanent Array: Installation of Electrodes in the Soil

[88] The electrodes used in this experiment are second-generation $Pb/PbCl_2$/kaolinite Petiau electrodes [*Petiau*, 2000]. They are installed in 1.2 to 1.5 m deep holes with a 40 cm diameter, and placed in 30 liters of salted kaolinite (Figure 5a). The volume of salted clay is protected by two horizontal plastic sheets from drainage induced by shallow water circulation. During the one-year Garchy experiment [*Perrier et al.*, 1997], this set-up was demonstrated to provide a stability of the order of 1 mV per year with a drift noise varying between 0.4 and 0.8 mV per month.

A.3. SP Temporary Arrays

[89] The measurement points of the temporary arrays consist in 60 cm long plastic tube with a 8 cm diameter, installed in a 50 cm deep hole (Figure 5b). Two liters of salted clay were inserted down each hole, following the installation method described by *Clerc et al.* [1998]. We also used for these measurements second-generation $Pb/PbCl_2$/kaolinite Petiau electrodes [*Petiau*, 2000]. Potential differences are measured with a high impedance voltmeter (input impedance larger than 20 M Ω).

A.4. Long-Term Stability of Electrodes

[90] The electric potential difference between the electrodes installed at the same measurement point can be measured at the station of the Sur-Frêtes ridge. Four sets of measurements have been performed since the beginning of the experiment (25 October 1995, 13 September 1996, 18 June 1998, and 25 November 1998). Detailed results are presented in *Trique* [1999].

[91] The electrodes located on the bottom of the lakes present long-term drifts, which amount to about 35 mV over 3 years. This indicates that the set-up of the electrodes for long-term measurement in water would need to be improved. For the electrodes installed in the soil, 24 of 27 $Pb/PbCl_2$/kaolinite electrodes have been checked. Seventy-six percent of them reveal drifts with amplitude smaller than 3 mV over three years. This confirms that the set up is satisfactory for long-term measurements in the soil. Electric potential changes of a few mV per month can be measured with reasonable accuracy with this technology.

A.5. Reliability of the Measured Seasonal Variations

[92] The reliability of the potential variations measured at some points can be studied using a loop residual, as mentioned above in the case of CH. For example, two loop residuals, obtained from the dipole combinations RCBB = BBE − BBW − BBG + BBR and RCLL = LLS + LGB − BBE − LRB, are also plotted in Figure 12 when they were available.

[93] The data indicate that RCBB is stable within better than 5 mV from November 1995 to February 1996, from October 1996 to December 1996, and from October 1997 to March 1998, indicating that the associated SP variations at LA are reliable within 5 mV during these periods (Figure 12). However, not enough loop residual RCLL data are available to check the electric potential variations at point RO. The dipole combination RCLL is stable within 5 mV only in December 1995 and from October to December 1996 but, during these periods, the variations of $V_{RO} - V_{BC}$ do not exceed 5 mV. In this case, the reproducibility of the observed variations over the years is particularly important to be able to trust the results.

[94] Similarly, on the La Gittaz side (Figure 13), the reliability of the SP variations is assessed only during the periods when the variations of RCBB is available and is observed to be smaller than 5 mV. In general, the number of residual loops of the continuous electric potential array of the experiment was not sufficient to assess the reliability of the measured electric potential variations over the whole observation period. For future experiments, it is recommended, when designing an electric potential array, to arrange the dipoles to provide a larger number of redundant closed loops.

[95] **Acknowledgments.** The authors thank the "Environment Program" of the Commissariat à l'Energie Atomique for support and the Ministry of Environment for a research grant. K. Spitzer is thanked for his help on the use of his numerical model. G. Petiau is thanked for his expertise and advice during the various stages of the experiment. P. Morat is thanked for numerous inspiring discussions. P. Tarits is thanked for initial guidance and for supporting one of the authors (S. Hautot). Last but not least, this manuscript was improved significantly thanks to the careful and detailed review by P. Roperch.

References

Adler, P. M., J. L. Le Mouël, and J. Zlotnicki, Electrokinetic and magnetic fields generated by flow through a fractured zone: a sensitivity study for La Fournaise volcano, *Geophys. Res. Lett.*, *26*, 795–798, 1999.

Aubert, M., and Q. Yéné Atangana, Self-potential method in hydrogeological exploration of volcanic areas, *Ground Water*, *34*, 1010–1016, 1996.

Aubert, M., Y. Nurrahmat Dana, and J. C. Dupuy, Application of the self-potential method to the detection of underground water courses in a volcanic area, *C. R. Acad. Sci.*, *312*, 325–330, 1991.

Bahr, K., Percolation in the crust derived from distortion of electric fields, *Geophys. Res. Lett.*, *27*, 1049–1052, 2000.

Bernard, P., Plausibility of long distance electrotelluric precursors to earthquakes, *J. Geophys. Res.*, *97*, 17,531–17,546, 1992.

Blake, E. W., and G. K. C. Clarke, Subglacial electrical phenomena, *J. Geophys. Res.*, *104*, 7481–7495, 1999.

Bogoslovsky, V. A., and A. A. Ogilvy, Natural potential anomalies as a quantitative index of the rate of seepage from water reservoirs, *Geophys. Prospect.*, *18*, 261–268, 1970.

Bogoslovsky, V. A., and A. A. Ogilvy, Geophysical methods for the investigation of landslides, *Geophysics*, *42*, 562–571, 1977.

Bogoslovsky, V. A., A. A. Ogilvy, and N. A. Strakhova, Magnetometric and electrometric methods for the investigation of the dynamics of landslide processes, *Geophys. Prospect.*, *25*, 280–291, 1977.

Clerc G., G. Petiau, and F. Perrier, The Garchy 1995–1996 electrode experiment technical report, technical report, INSU–CNRS/CEA, Paris, 1998.

Corwin, R. F., and D. B. Hoover, The self-potential method in geothermal exploration, *Geophysics*, *44*, 226–245, 1979.

Corwin, R. F., and H. F. Morrison, Self-potential variations preceding earthquakes in central California, *Geophys. Res. Lett.*, *4*, 171–174, 1977.

Egbert, G. D., J. R. Booker, and A. Schultz, Very long period magnetotellurics at Tucson Observatory: Estimation of impedances, *J. Geophys. Res.*, *97*, 15,113–15,128, 1992.

Electricité de France, Service Géologie, *Note géologique sur l'étanchéité de la cuvette de Roselend en direction du col de Sur-Frêtes, Rep. 1-12*, Paris, 1951.

Ernsson K., and H. U. Scherer, Self-potential variations with time and their relation to hydrogeologic and meteorological parameters, *Geophysics*, *51*, 1967–1977, 1986.

Fujinawa, Y., T. Kumagai, and K. Takahashi, A study of anomalous underground electric field variations associated with a volcanic eruption, *Geophys. Res. Lett.*, *19*, 9–12, 1992.

Geller, R., (Ed.), Debate on ≪VAN≫, Special issue, *Geophys. Res. Lett.*, 23, 1291–1452, 1996.

Geller, R. J., Earthquake prediction, a critical review, *Geophys. J. Int.*, *131*, 425–450, 1997.

Gensane, O., B. Konyukhov, J. L. Le Mouël, and P. Morat, SP coseismic signals observed on an electrodes array in an underground quarry, *Geophys. Res. Lett.*, *26*, 3529–3532, 1999.

Gex, P., Phénomènes d'électrofiltration liés à quelques sites de barrages, *Bull. Soc. Vaudoise Sci. Nat.*, *75*, 39–50, 1980.

Gex, P., Les phénomènes de polarisation spontanée liés à la zone houillère des environs de Chandonne, Val d'Entremont (Valais), *Bull. Soc. Vaudoise Sci. Nat.*, *76*, 33–46, 1982.

Harvey, F. E., D. R. Lee, D. L. Rudolph, and S. K. Frape, Locating groundwater discharge in large lakes using bottom sediment electrical conductivity mapping, *Water Resour. Res.*, *33*, 2609–2615, 1997.

Hashimoto, T., and Y. Tanaka, A large self-potential anomaly on Unzen volcano, Shimabara Peninsula, Kyushu Island, Japan, *Geophys. Res. Lett.*, *22*, 191–194, 1995.

Hautot S., P. Tarits, F. Perrier, C. Tarits, and M. Trique, Groundwater electromagnetic imaging in complex geological and topographical regions: A case study of a tectonic boundary in the French Alps, *Geophysics*, *67*, 1048–1060, 2002.

Ishido, T., and H. Mizutani, Experimental and theoretical basis of electrokinetic phenomena in rock-water systems and its applications to geophysics, *J. Geophys. Res.*, *26*, 1763–1775, 1981.

Ishido, T., T. Kikuchi, N. Matsushima, Y. Yano, S. Nakao, M. Sugihara, T. Tosha, S. Takakura, and Y. Ogawa, Repeated self-potential profiling of Izu-Oshima volcano, Japan, *J. Geomagn. Geoelectr.*, *49*, 1267–1278, 1997.

Janod, A., L'aménagement de Roselend, *Construction*, *12*, 291–298, 1957.

Jones, A. G., Static shift of magnetotelluric data and its removal in a sedimentary basin environment, *Geophysics*, *53*, 967–978, 1988.

Jouniaux, L., and J. P. Pozzi, Permeability dependence of streaming potential in rocks for various fluid conductivities, *Geophys. Res. Lett.*, *22*, 485–488, 1995a.

Jouniaux, L., and J. P. Pozzi, Streaming potential and permeability of saturated sandstones under triaxial stress: Consequences for electrotelluric anomalies prior to earthquakes, *J. Geophys. Res.*, *100*, 10,197–10,209, 1995b.

Jouniaux, L., M. L. Bernard, J. P. Pozzi, and M. Zamora, Streaming potential in volcanic rocks from Mount Pelée, *J. Geophys. Res.*, *105*, 8391–8401, 2000.

Koizumi, N., E. Tsukuda, O. Kamigaichi, N. Matsumoto, M. Takahashi, and T. Sato, Preseismic changes in groundwater level and volumetric strain associated with earthquake swarms off the east coast of the Izu Peninsula, Japan, *Geophys. Res. Lett.*, *26*, 3509–3512, 1999.

Le Mouël, J. L., and M. Menvielle, Geomagnetic variation anomalies and

deflection of telluric currents, *Geophys. J. R. Astron. Soc.*, *68*, 575–587, 1982.

Lénat, J. F., B. Robineau, S. Durand, and P. Bachèlery, A self-potential survey of the summit zone of Karthala volcano, *C. R. Acad. Sci.*, *327*, 781–788, 1998.

Lighthill J. (Ed.), *A Critical Review of VAN, Earthquake Prediction From Seismic Electrical Signals*, World Sci., Singapore, 1996.

Lorne, B., F. Perrier, and J. P. Avouac, Streaming potential measurements, 1, Properties of the electrical double layer from crushed rock samples, *J. Geophys. Res.*, *104*, 17,857–17,877, 1999a.

Lorne, B., F. Perrier, and J. P. Avouac, Streaming potential measurements, 2, Relationship between electrical and hydraulic flow patterns from rock samples during deformation, *J. Geophys. Res.*, *104*, 17,879–17,896, 1999b.

Malengreau, B., J. F. Lénat, and A. Bonneville, Cartography and temporal observation of self-potential anomalies at Piton de la Fournaise, *Bull. Soc. Geol. Fr.*, *165*, 221–232, 1994.

Menvielle, M., and P. Tarits, 2-D or 3-D interpretation of conductivity anomalies: Example of the Rhine-Graben conductivity anomaly, *Geophys. J. R. Astron. Soc.*, *84*, 216–226, 1986.

Michel, S., and J. Zlotnicki, Self-Potential and magnetic surveying of La Fournaise volcano (Réunion Island): Correlations with faulting, fluid circulations, and eruption, *J. Geophys. Res.*, *103*, 17,845–17,857, 1998.

Mizutani, H., T. Ishido, T. Yokokura, and S. Ohnishi, Electrokinetic phenomena associated with earthquakes, *Geophys. Res. Lett.*, *3*, 365–368, 1976.

Morat, P., and J. L. Le Mouël, Electrical signals generated by stress variations in porous non saturated rocks, *C. R. Acad. Sci.*, *315*, 955–963, 1992.

Morat, P., J. L. Le Mouël, and J. Zlotnicki, Electrical signals generated by the collapse of the pillars of a gypsum quarry, *C. R. Acad. Sci.*, *308*, 33–38, 1989.

Morgan, F. D., E. R. Williams, and T. R. Madden, Streaming potential properties of westerly granite with applications, *J. Geophys. Res.*, *94*, 12,449–12,461, 1989.

Muir-Wood, R., and G. C. P. King, Hydrological signatures of earthquake strain, *J. Geophys. Res.*, *98*, 22,035–22,068, 1993.

Noir, J., E. Jacques, P. Tapponnier, and G. King, Fluid flow triggered migration of events in the 1989 Dobi earthquake sequence of Central Afar, *Geophys. Res. Lett.*, *24*, 2335–2338, 1997.

Nur, A., and J. R. Booker, Aftershocks caused by fluid flow, *Science*, *175*, 885–887, 1972.

Ogilvy, A. A., M. A. Ayed, and V. A. Bogoslovsky, Geophysical studies of water leakages from reservoirs, *Geophys. Prospect.*, *17*, 36–62, 1969.

Park, S. K., Monitoring changes of resistivity prior to earthquakes in Parkfield, California, with telluric arrays, *J. Geophys. Res.*, *96*, 14,221–14,237, 1991.

Park, S. K., Monitoring resistivity change in Parkfield, California: 1988–1995, *J. Geophys. Res.*, *102*, 24,545–24,559, 1997.

Park, S. K., and D. V. Fitterman, Sensitivity of the telluric monitoring array in Parkfield, California, to changes of resistivity, *J. Geophys. Res.*, *95*, 15,557–15,571, 1990.

Park, S. K., M. J. S. Johnston, T. R. Madden, and H. F. Morrison, Electromagnetic precursors to earthquakes in the ULF band: A review of observations and mechanisms, *Rev. Geophys.*, *31*, 117–132, 1993.

Perrier, F., and P. Morat, Characterization of electrical daily variations induced by capillary flow in the non-saturated zone., *Pure Appl. Geophys.*, *157*, 785–810, 2000.

Perrier, F., et al., A one-year systematic study of electrodes for long period measurement of the electric field in geophysical environments, *J. Geomagn. Geoelectr.*, *49*, 1677–1696, 1997.

Perrier, F., M. Trique, B. Lorne, J. P. Avouac, S. Hautot, and P. Tarits, Electric potential variations associated with yearly lake level variations, *Geophys. Res. Lett.*, *25*, 1955–1958, 1998.

Perrier, F., M. Trique, J. Aupiais, U. Gautam, and P. Shrestha, Electric potential variations associated with periodic spring discharge in western Nepal, *C. R. Acad. Sci.*, *328*, 73–79, 1999.

Petiau, G., Second generation of lead-lead chloride electrodes for geophysical applications, *Pure Appl. Geophys.*, *157*, 357–382, 2000.

Raleigh, B., P. Molnar, T. Hanks, A. Nur, J. Savage, H. Craig, R. Turner, and G. Bennett, The prediction of the Haicheng earthquake, *Eos Trans. AGU*, *58*, 236–272, 1977.

Revil, A., and P. A. Pezard, Streaming electrical potential anomaly along faults in geothermal areas, *Geophys. Res. Lett.*, *25*, 3197–3200, 1998.

Revil, A., P. A. Pezard, and E. W. J. Glover, Streaming potential in porous media, 1, Theory of the zeta potential, *J. Geophys. Res.*, *104*, 20,021–20,031, 1999a.

Revil, A., H. Schwaeger, L. M. Cathles III, and P. D. Manhardt, Streaming potential in porous media, 2, Theory and application to geothermal systems, *J. Geophys. Res.*, *104*, 20,033–20,048, 1999b.

Roeloffs, E. A., Hydrologic precursors to earthquakes: A review, *Pure Appl. Geophys.*, *126*, 177–209, 1988.

Sasai, Y., J. Zlotnicki, Y. Nishida, P. Yvetot, P. Morat, H. Murakami, Y. Tanaka, Y. Ishikawa, S. Koyama, and W. Sekiguchi, Electromagnetic monitoring of Miyake-jima volcano, Izu-Bonin arc, Japan: A preliminary report, *J. Geomagn. Geoelectr.*, *49*, 1293–1316, 1997.

Sasai, Y., J. Zlotnicki, Y. Nishida, M. Uyeshima, P. Yvetot, Y. Tanaka, H. Watanabe, and Y. Takahashi, Evaluation of electric and magnetic field monitoring of Miyake-jima volcano (Central Japan): 1995–1999, *Ann. Geofis.*, *44*, 239–260, 2001.

Scholz, C. H., L. R. Sykes, and Y. P. Aggarwal, Earthquake prediction: A physical basis, *Science*, *181*, 803–810, 1973.

Spitzer, K., A 3-D finite-difference algorithm for DC resistivity modeling using conjugate gradient methods, *Geophys. J. Int.*, *123*, 903–914, 1995.

Stoll, J., J. Bigalke, and E. W. Grabner, Electrochemical modeling of self-potential anomalies, *Surv. Geophys.*, *16*, 107–120, 1995.

Thony, J. L., P. Morat, G. Vachaud, and J. L. Le Mouël, Field characterization of the relationship between electrical potential gradients and soil water flux, *C. R. Acad. Sci.*, *325*, 317–321, 1997.

Trique M., Etude en site naturel des phénomènes physiques associés au cycle sismique: l'expérience de Sur-Frêtes, doctoral thesis, Univ. Joseph Fourier, Grenoble, France, 1999.

Trique, M., P. Richon, F. Perrier, J. P. Avouac, and J. C. Sabroux, Radon emanation and electric potential variations, associated with transient deformation near reservoir lakes, *Nature*, *399*, 137–141, 1999.

Varotsos, P., K. Alexopoulos, and M. Lazaridou, Latest aspects of earthquake prediction in Greece by seismic electric signals, II, *Tectonophysics*, *224*, 1–37, 1993.

Varotsos, P., N. Sarlis, and M. Lazaridou, Interconnection of defect parameters and stress-induced electric signals in ionic crystals, *Phys. Rev. B*, *59*, 24–27, 1999.

Yoshida, S., O. C. Clint, and P. R. Sammonds, Electric potential changes prior to shear fracture in dry and saturated rocks, *Geophys. Res. Lett.*, *25*, 1577–1580, 1998.

Zhdanov, M. S., and G. V. Keller, The geoelectrical methods in geophysical exploration, Elsevier Sci., New York, 1994.

Zlotnicki, J., and J. L. Le Mouel, Volcanomagnetic effects observed on Piton de la Fournaise Volcano (Reunion Island): 1985–1987, *J. Geophys. Res.*, *93*, 9157–9171, 1988.

Zlotnicki, J., and J. L. Le Mouël, Possible electrokinetic origin of large magnetic variations at La Fournaise Volcano, *Nature*, *343*, 633–636, 1990.

Zlotnicki, J., S. Michel, and C. Annen, Self-potential anomalies and convective systems on La Fournaise volcano (Réunion Island, France), *C. R. Acad. Sci.*, *318*, 1325–1331, 1994.

Zlotnicki, J., J. L. Le Mouël, Y. Sasai, P. Yvetot, and M. H. Ardisson, Self-potential changes associated with volcanic activity. Short-term signals associated with March 9, 1998 eruption on La Fournaise volcano (Réunion Island), *Ann. Geofis.*, *44*, 335–354, 2001.

Zohdy, A. A. R., L. A. Anderson, and L. J. P. Muffler, Resistivity, self-potential, and induced-polarization surveys of a vapor-dominated geothermal system, *Geophysics*, *38*, 1130–1144, 1973.

M. Trique, European Patent Office, Erhardtstrasse 27, G-80331 Munich, Germany. (mtrique@epo.org)

J.-P. Avouac, T. Froidefond, and F. Perrier, Département Analyse, Surveillance, Environnement, Commissariat à l'Energie Atomique, B.P.12, F-91680 Bruyères-Le-Châtel, France.

S. Hautot, UMR 6538 "Domaines Océaniques", IUEM Technopole Brest-Iroise, Place Nicolas Copernic, 29280 Plouzané, France.

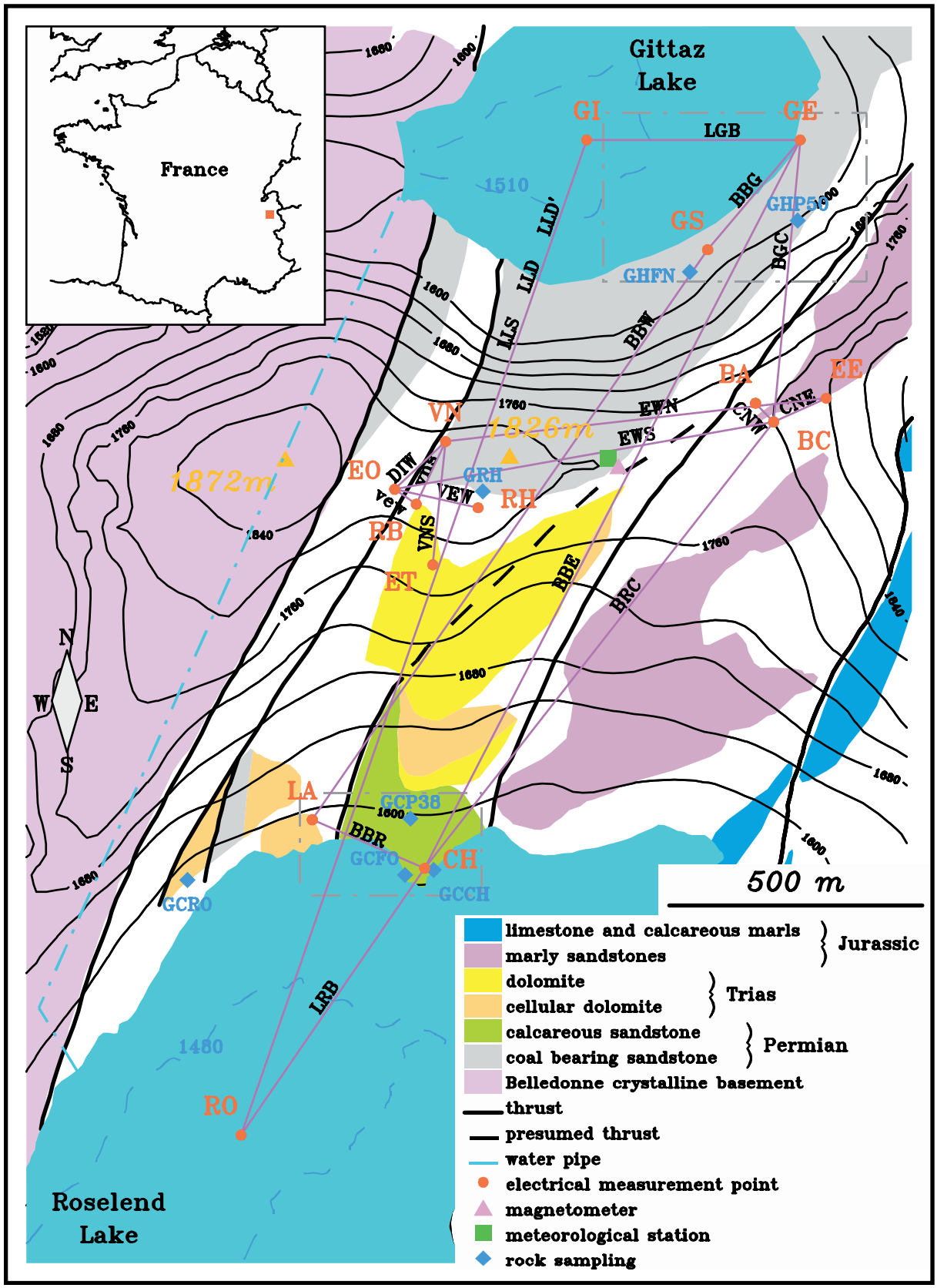

Figure 1. Map of the Sur-Frêtes ridge with the main geological units and the permanent SP monitoring array. The locations of rocks sampled for laboratory measurements are also indicated.

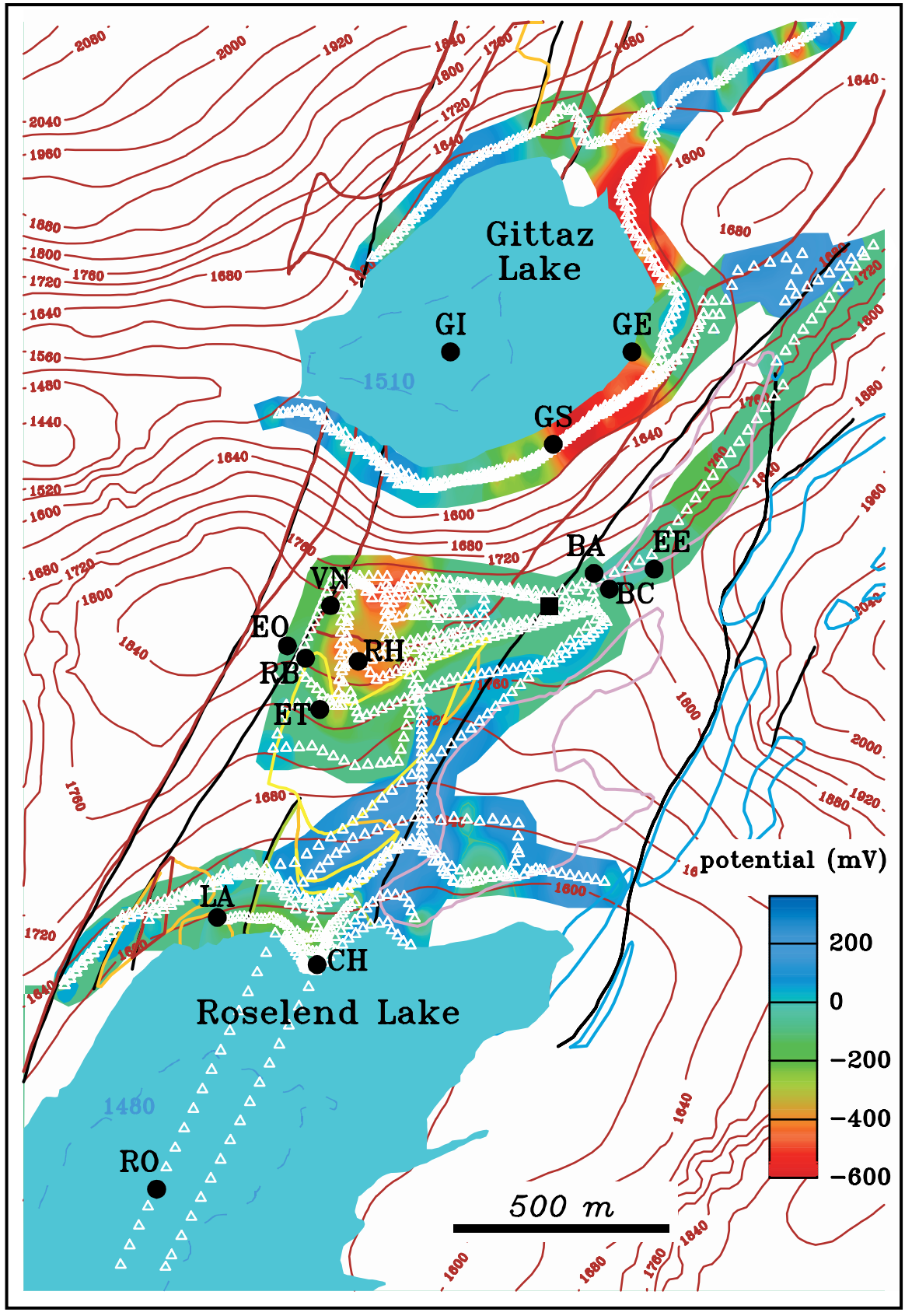

Figure 2. Map of the static SP distribution. The SP measurement points are indicated by white triangles (approximately a total of 1300 points). The contours of the main geological units are displayed using the color code defined in Figure 1. The reference point for the SP mapping is represented by a black square. The black dots represent the measurement points of the permanent SP monitoring array.

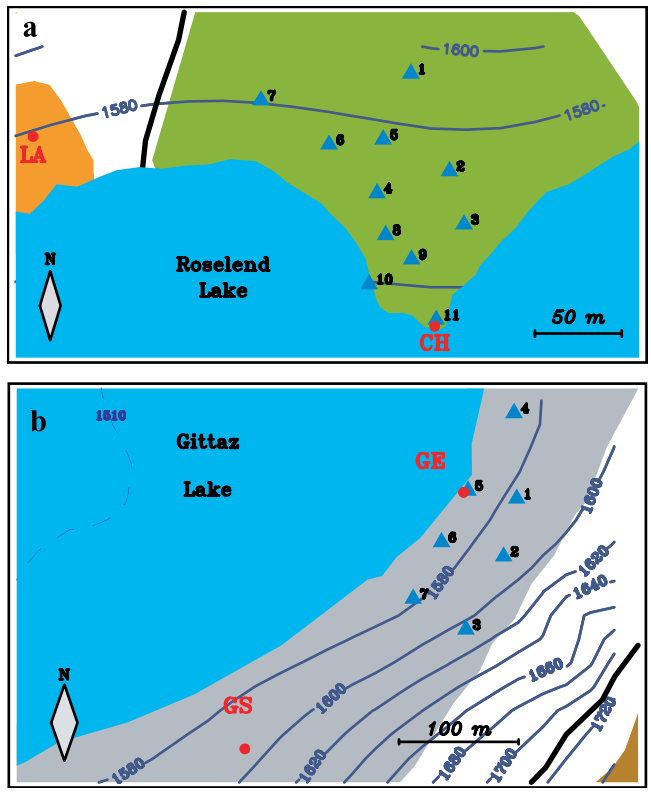

Figure 6. Layout of the temporary electric potential arrays on the Roselend (a) and La Gittaz side (b). One point of each temporary array is located near a point of the permanent array, so that all SP measurements can be referred to the BC reference point on the Sur-Frêtes ridge (Figure 1).